Science Advances
AAAS

Supplementary Materials for

The large role of declining atmospheric sulfate deposition and rising CO_2 concentrations in stimulating future wetland CH_4 emissions

Lu Shen *et al.*

Corresponding author: Lu Shen, lshen@pku.edu.cn

Sci. Adv. **11**, eadn1056 (2025)
DOI: 10.1126/sciadv.adn1056

The PDF file includes:

Supplementary Text S1 to S3
Figs. S1 to S29
Tables S1 to S6
Legends for data S1 to S3
References

Other Supplementary Material for this manuscript includes the following:

Data S1 to S3

Text S1. Constructing the statistical model to predict meteorological effects on wetland emissions

Wetland methane fluxes from a specific gridcell often show strong correlations not only with local meteorology, but also with the meteorological variables in the surrounding regions. For example, in many cases (Fig. S1), regions with statistically significant correlations follow the network of rivers. These spatial correlation patterns should help improve the predictive capability of a statistical model that just relies on local meteorology as covariates.

Here, following Shen et al.(*81*), we construct the regional climate patterns driving wetland methane fluxes through the use of singular value decompositions (SVDs) of the spatial correlations between methane emissions in each grid box and meteorological variables (T and P) in the surrounding region (~1000 km). The spatial correlations of these two variables, as demonstrated in Fig. S1, include information that can be stored in a 20 × 20 × 2 (longitude × latitude × variable) matrix or a 400× 2 matrix if we align the longitude and latitude into one dimension (denoted as $\boldsymbol{F}$ here). To effectively compress the information of this multidimensional matrix, we adopt the SVD method, which proceeds as follows:

$$\boldsymbol{F} = \boldsymbol{U}\boldsymbol{L}\boldsymbol{V}^{\mathrm{T}} \quad \text{(Eq. S1)}$$

where $\boldsymbol{L}$ is a diagonal matrix with non-negative numbers on the diagonal. Each column of the right matrix of SVD, or $\boldsymbol{V}$, represents the weights of T and P, representing the variable importance of each mode. Each column of the right matrix, or $\mathbf{U}$, represents the spatial weights of the corresponding mode. For example, Fig. S2a-b shows the spatial and variable weights of the 1st SVD (SVD1) mode for the spatial information presented in Fig. S1, and this mode explains 70 % of the total variance. The spatial weights highly resemble the correlation pattern regarding P in Fig S1b. The corresponding variable weights reveal that precipitation is the dominant factor in this mode. In the 2nd SVD mode, temperature is the dominating factor, and the spatial weights show similar distribution with that in Fig. S1a, and. We repeat this exercise for each wetland pixel.

For new meteorological fields, we can calculate each of the regional climate patterns using the inverse process of Eq. S1. Before this, we scale the time series of each variable in each gridbox to have zero mean and unit standard deviation. Here, we define this matrix for every month t, after being preprocessed, as $\boldsymbol{M}_{\mathrm{t}}$, which includes the standardized meteorological variables P and T for a specific month t. The magnitude of each SVD mode is then calculated using the inverse process of SVD, written as

$$S_k = \boldsymbol{U}_{\mathbf{k}}^{\mathrm{T}}\boldsymbol{M}_{\mathrm{t}}\boldsymbol{V}_{\mathbf{k}} \quad \text{(Eq. S2)}$$

where $\boldsymbol{U}_{\boldsymbol{k}}$ refers to the k^{th} column in the spatial weights matrix $\boldsymbol{U}$, $\boldsymbol{V}_{\mathbf{k}}$ to the k^{th} column in the variable weights matrix $\boldsymbol{V}$**,** and S_{k} is a scalar depicting the magnitude of the k^{th} SVD mode of the new meteorological field $\boldsymbol{M}_{\mathrm{t}}$ for that month. The scales S_{k} is used as a predictor in the multivariate linear regression model in Eq. 3 and 4 (see Methods for details)

To avoid unrealistically extreme values predicted by statistical approaches (Eq. 3-4 in main text), we determine the upper bound at different climate zones as follows. We first normalize monthly CH_4 emissions for each pixel by dividing data with 2000-2019 mean emissions, denoted as E_m. This process can factor out the effect of the absolute magnitude of emissions observed across pixels. Gridcells are classified in classes of annual mean temperature T_{mC} of the period 2000-2019, with bin size set to 2°C. For pixels falling in a given temperature class (T_{mC}), we calculate E_m^{99th} as the 99th percentile of all E_m. For a specific pixel i in the class of T_{mC}, its upper bound of methane emissions is determined as $\gamma \overline{f}_i E_m^{99th}$, where $\overline{f}_i$ is the mean value of wetland CH_4 emissions in this pixel. In this work, γ is assumed to be 5, and the percentage of gridcells reaching the upper bound is <0.01% in ssp119 and ~0.05% in ssp585. The predicted 2000-2100 changes of emissions diff by <9% if γ increases from 3 to 10.

Text S2. Suppressive effects of sulfate on methane formation

Methanogenesis in the anoxic environment is the primary pathway to produce CH_4, using hydrogen, carbon dioxide and acetate as substrates(*87*). In the presence of an excess of sulfate, sulfate-reducing bacteria (SRB) compete with methanogens for the common substrates (hydrogen and acetate) (*58*, *88*), using sulfate as a terminal electron acceptor to degrade organic compounds (*58*). Importantly, the SRBs can easily out-compete methanogens(*58*), thus suppressing the gross CH_4 formation (*16*, *58*, *87*).

Methanogenic reactions(*58*)

$$4H_2 + HCO_3^- + H^+ \rightarrow CH_4 + 3H_2O$$

$$\text{Acetate}^- + H_2O \rightarrow CH_4 + HCO_3^-$$

Sulphate-reducing reactions (*58*)

$$4H_2 + SO_4^{2-} + H^+ \rightarrow HS^- + 4H_2O$$

$$\text{Acetate}^- + SO_4^{2-} \rightarrow HS^- + 2HCO_3^-$$

$$\text{Other oranigc acids} + SO_4^{2-} \rightarrow \text{Acetate}^- + HS^- + 2HCO_3^-$$

1.1 **Text S3. Future projection of wetland area**

Only a limited number of CMIP6 models provide archives of wetland areas. Here, we select these models based on two criteria: (1) the model should include all Tier-1 climate scenarios (ssp126, ssp245, ssp37, and ssp585) to provide a full spread of sensitivity to radiative forcing, and (2) the global wetland area is in the normal range of 1-20 million km^2 (*89*). Finally, we identified 5 models, including CanESM5, CESM2, CESM2-WACCM, NorESM2-LM, and NorESM2-MM. Among these models, only CanESM5 provides outputs for all the historical and 7 future climate scenarios. The wetland area in these models also differs by 45%, ranging from 4.4 to 6.4 million km^2. Thus, to avoid bias in model selection and to fully account for the uncertainty inherent in these models, we first estimate the wetland area of the missing scenarios using a simple linear interpolation based on those of nearest radiative forcing:

$$A_{ssp119} = 1.37A_{ssp126} - 0.37A_{ssp245}$$

$$A_{ssp434} = 0.58A_{ssp126} + 0.42A_{ssp245}$$

$$A_{ssp460} = 0.60A_{ssp370} + 0.40A_{ssp245}$$

From 2000-2100, global wetland area, derived from 5 CMIP6 models, remains largely unchanged (-3% to 5%) in low-CO_2 scenarios (ssp119, ssp126), and increases by ~10% with large discrepancies across models (5-25%) in ssp585 (Fig. S28-29). Tropical wetlands are estimated to become drier in the future climate, resulting in declining extents (Fig. S28-S29). Conversely, northern mid- to high-latitude wetlands are expected to increase by ~20% in ssp585.

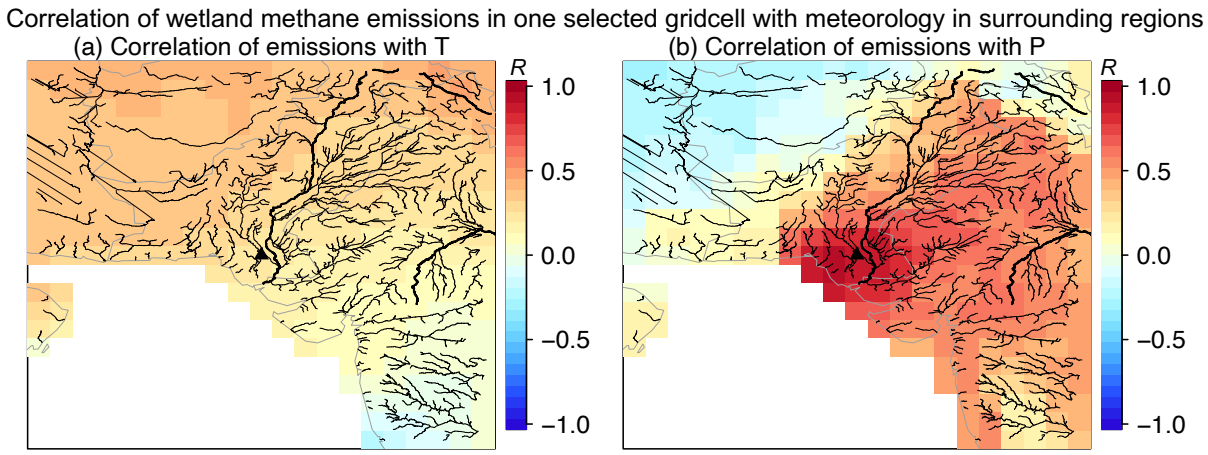


Fig. S1. **Correlations of methane fluxes in one selected gridcell (denoted as the black triangle) with meteorological variables in surrounding regions**. Panels shows monthly correlations with (a) temperature and (b) precipitation from 2001-2019. The river network is overlayed with maps(*90*).

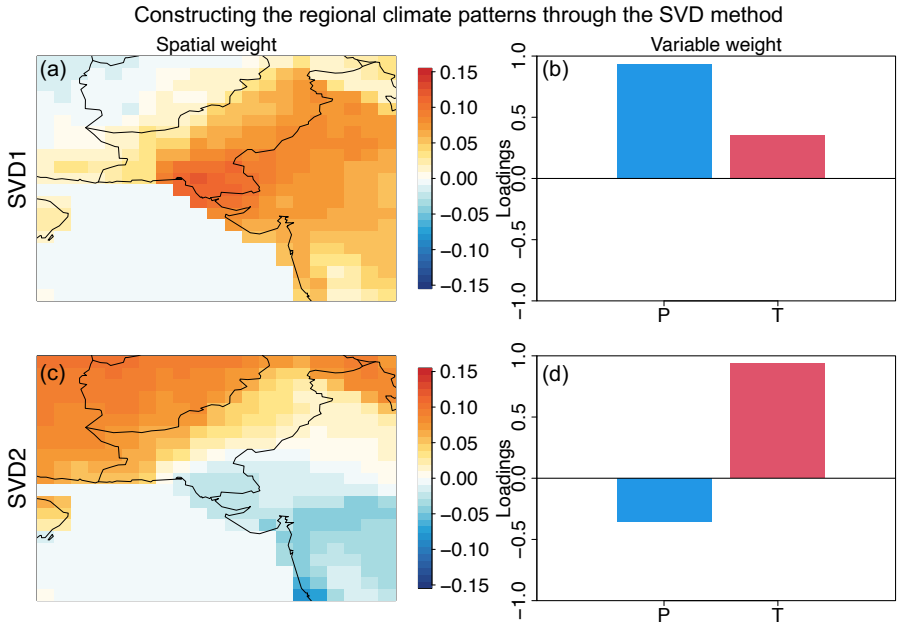


Fig. S2. **Spatial and variable weights of the SVD method**. The top panel shows the spatial and variable weights for the 1st singular value decomposition (SVD) modes. The spatial weight refers to the first column of the right matrix, or ***U***, in Equation S1, representing the importance of this weighting in different gridcells. The variable weights represent the variable importance of this mode, denoted as the first column of the right matrix of SVD, or **V**.

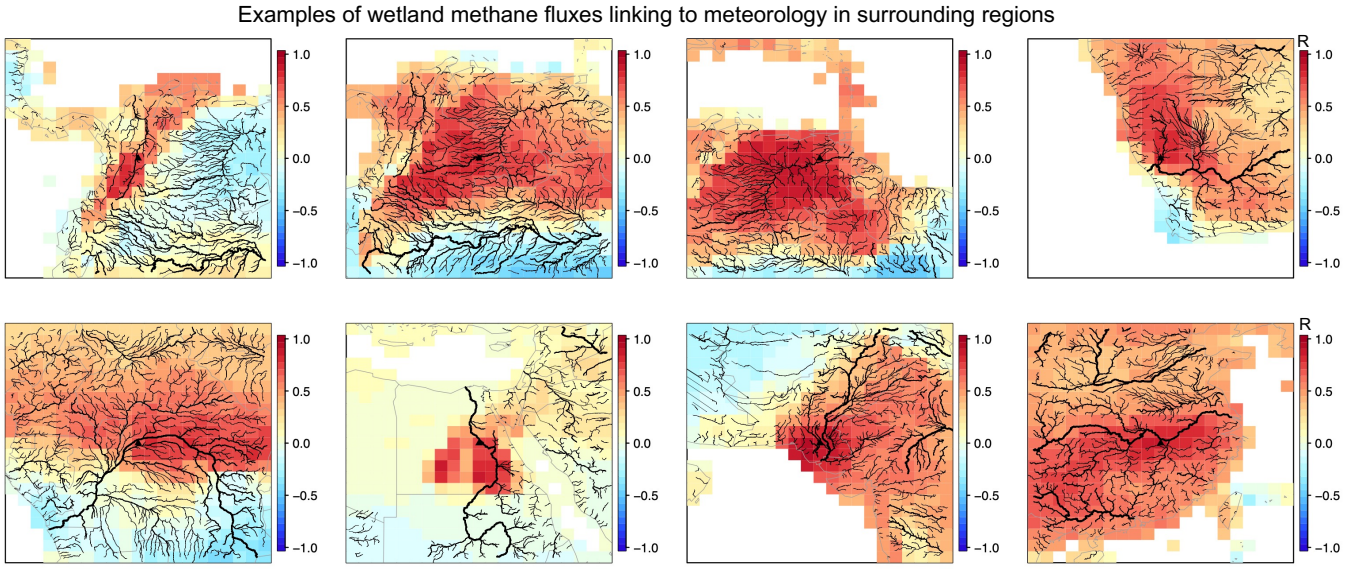


Fig. S3. **Correlations of monthly wetland methane emission in one selected gridcell (the triangle in each panel) with precipitation in all surrounding regions**. The river network is overlayed with maps(*90*). These patterns clearly show that wetland fluxes are linked to precipitation in the upstream rivers and regions.

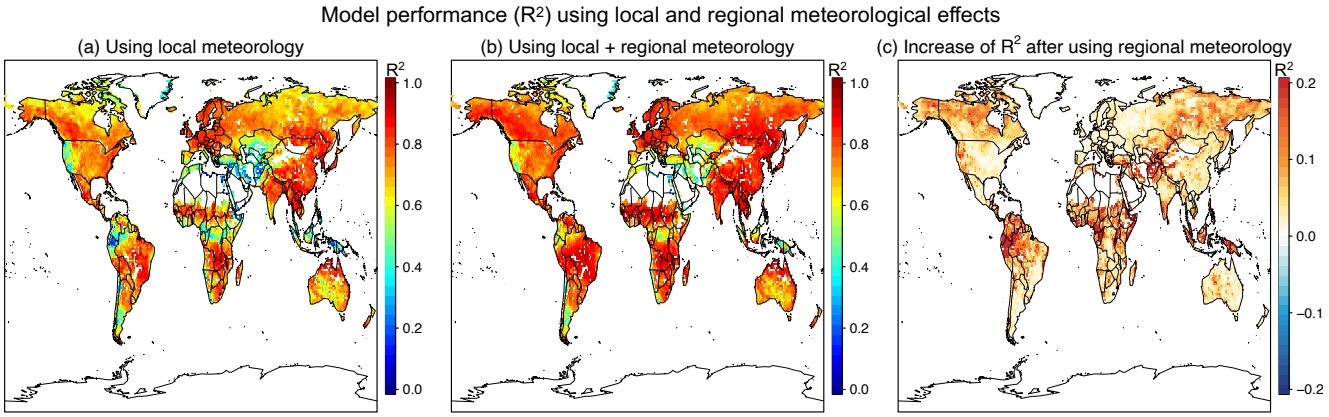


Fig. S4. **Effects of meteorological effects in improving the predicative capability**. (a) The correlation of determination (R^2) from using only local meteorology. (b) Same as (a) but for using both local meteorology and regional climate patterns. (c) The increment of R^2 from adding regional climate patterns in the linear regression model.

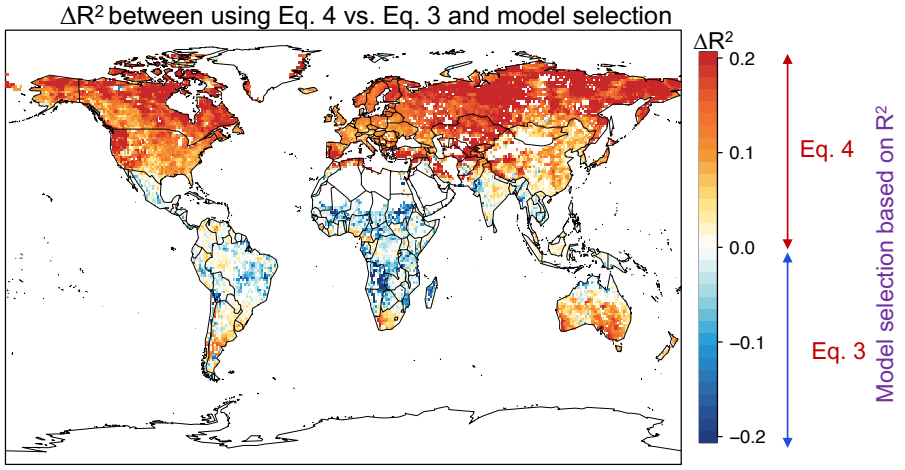


Fig. S5. Difference in R^2 using Eq. 3 vs. Eq. 4. For each pixel, we fit the data with both models and select the one with higher R^2. According to this figure, we select Eq. 4 in gridcells with red colors and Eq. 3 with blue colors. Here, this figure denotes the result in one process-based model from WetCHARTs.

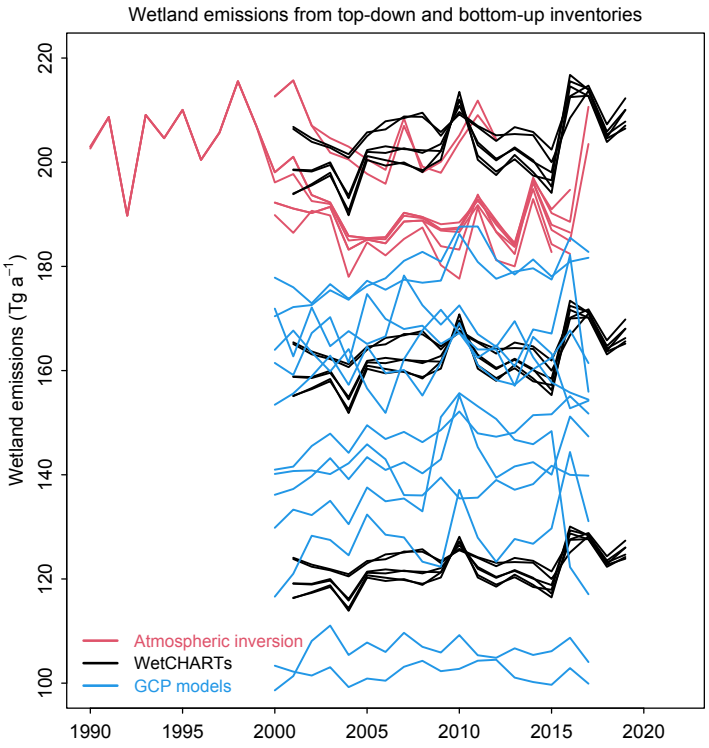


Fig. S6. **Timeseries of global wetland methane emissions from 1990 to 2019**. Inventories include those from using top-down and bottom-up approaches (see Table S1 for more details).

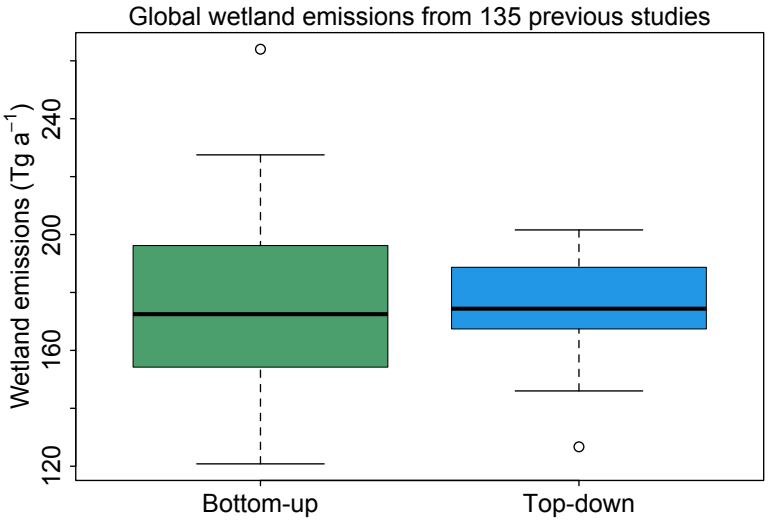


Fig. S7. **Global wetland methane emissions from bottom-up vs. top-down approaches from 135 previous studies** (Data S1). The top and bottom of the box are the 25th and 75th percentiles, the vertical bars are for the 5th and 90th percentiles, and the center line is the 50th percentile.

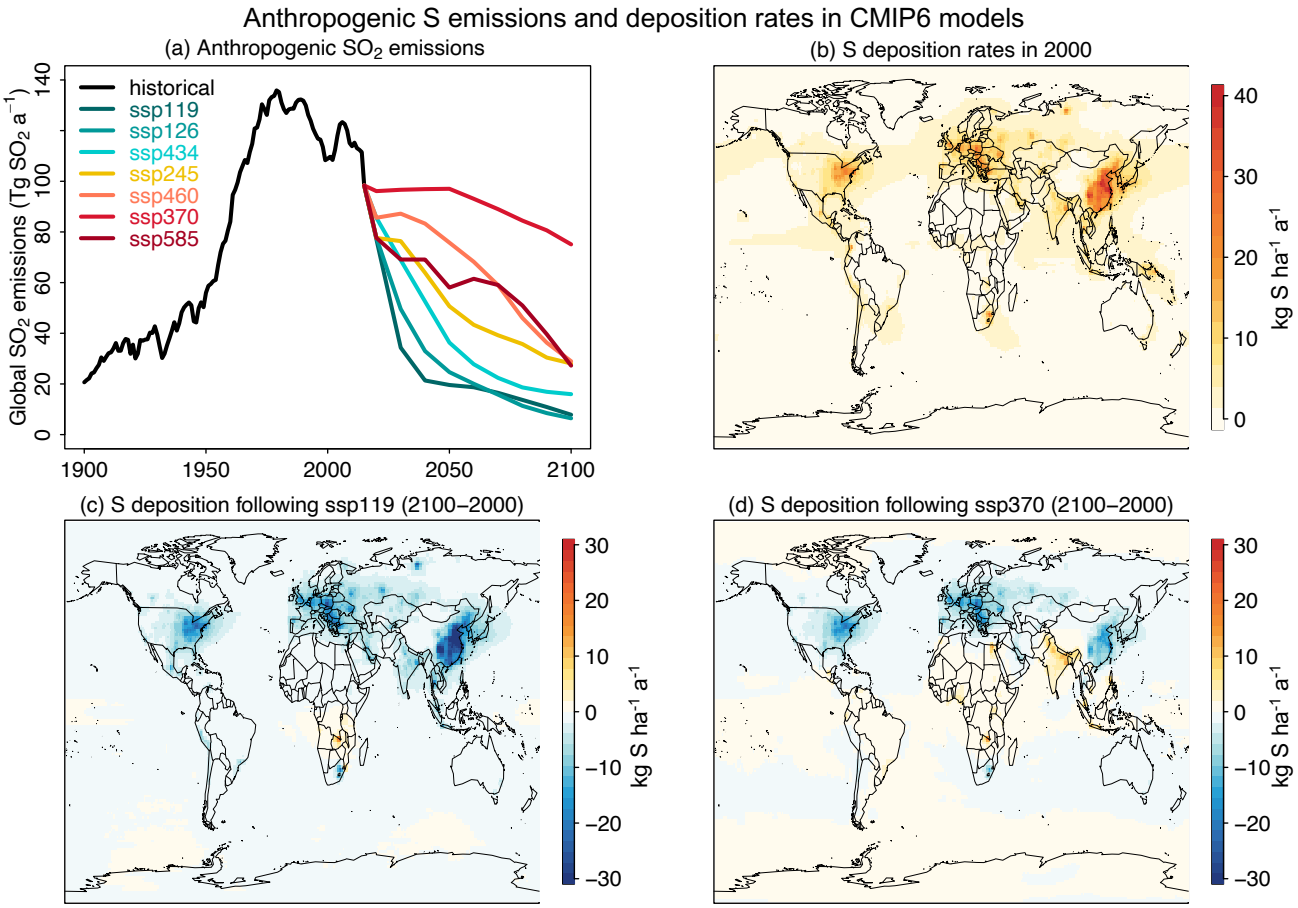


Fig. S8. **Anthropogenic SO_2 emissions and future changes of sulfate deposition rates in different scenarios**. (a) Global anthropogenic SO_2 emissions from 1900-2100 used in AerChemMIP models. (b) Global average S deposition rates in 2000, averaged from 4 CMIP6 models (see Table S3 for more details). (c) Changes of S deposition rates in the ssp119 scenario from 2000-2100. (d) Same as (b) but for the ssp585 scenario.

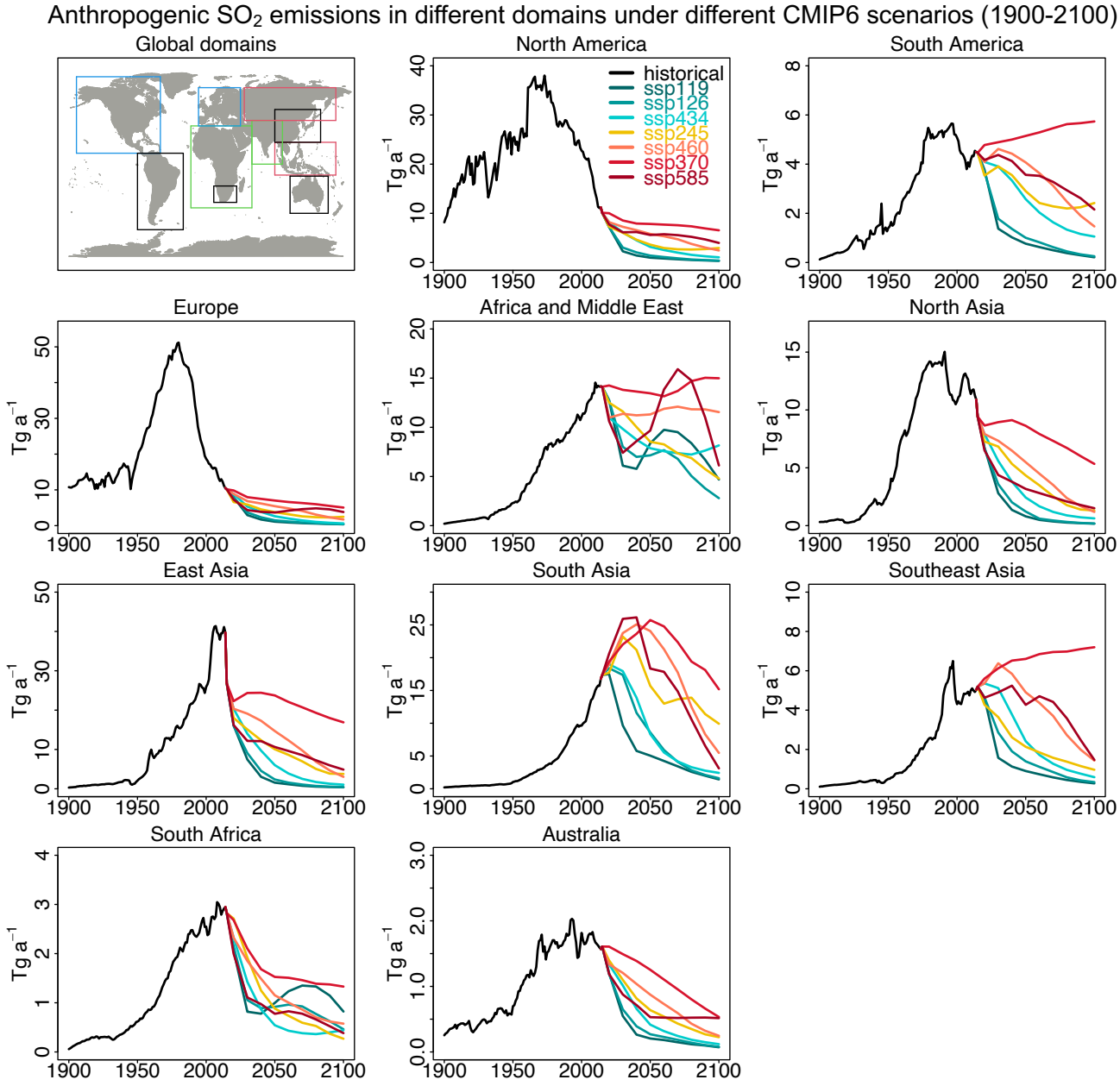


Fig. S9. **Anthropogenic SO_2 emissions in different domains under different CMIP6 scenarios**. The data used in this figure is from Durack et al. (*38*)

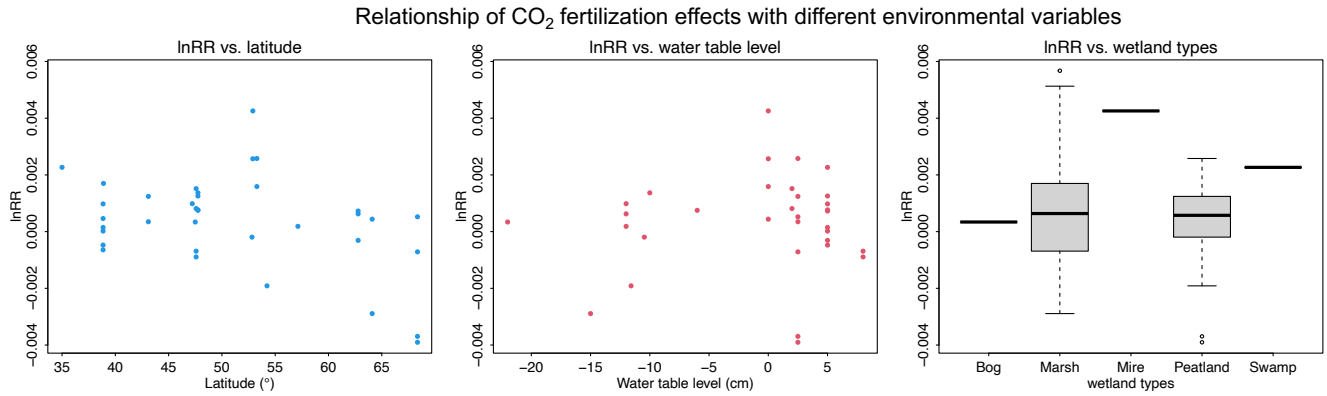


Fig. S10. **Relationship of ln*RR* (the natural log of the response ratio) with different covariates, including latitudes, water table levels and wetland types**. The data is from Data S2. The equation for ln*RR* can be found in Eq. 2.

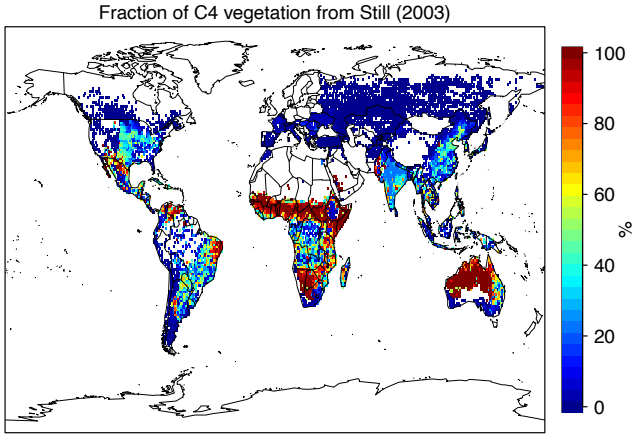


Fig. S11. **The global distribution of the faction of C4 plants** (Still et al.(*62*)). Ganesan et al.(*91*) demonstrated that the wetland $\delta^{13}C(CH4)$ source signature based on this C4 distribution map can match the signatures derived from atmospheric observations.

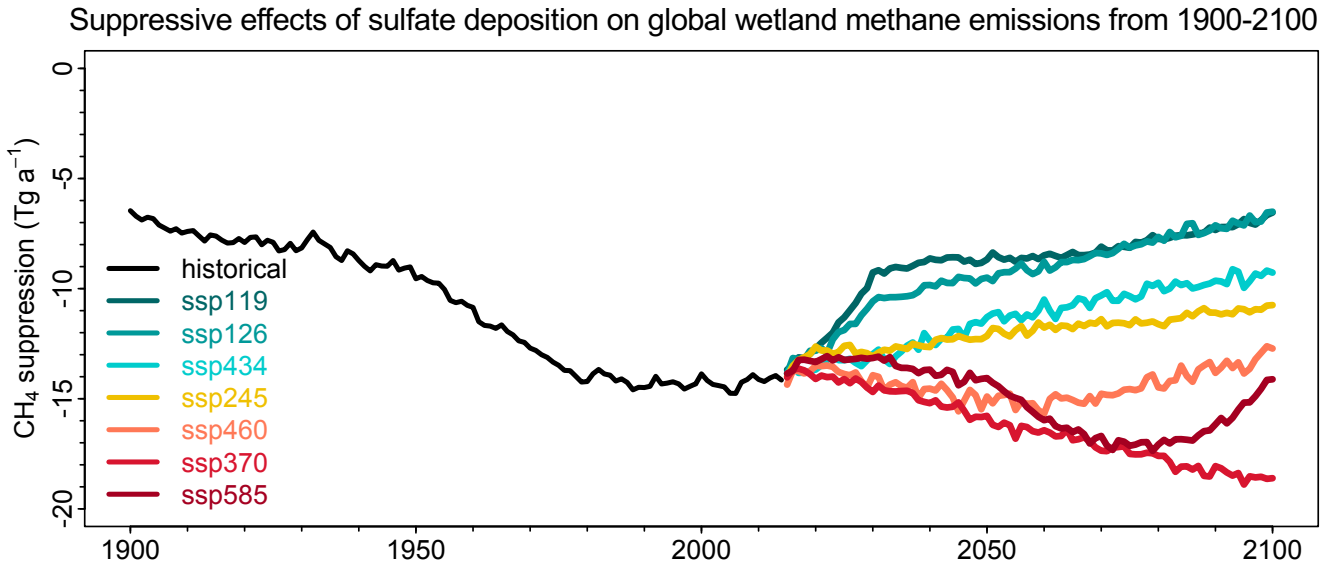


Fig. S12. The suppressive effects of sulfate deposition on global wetland emissions along different climate scenarios.

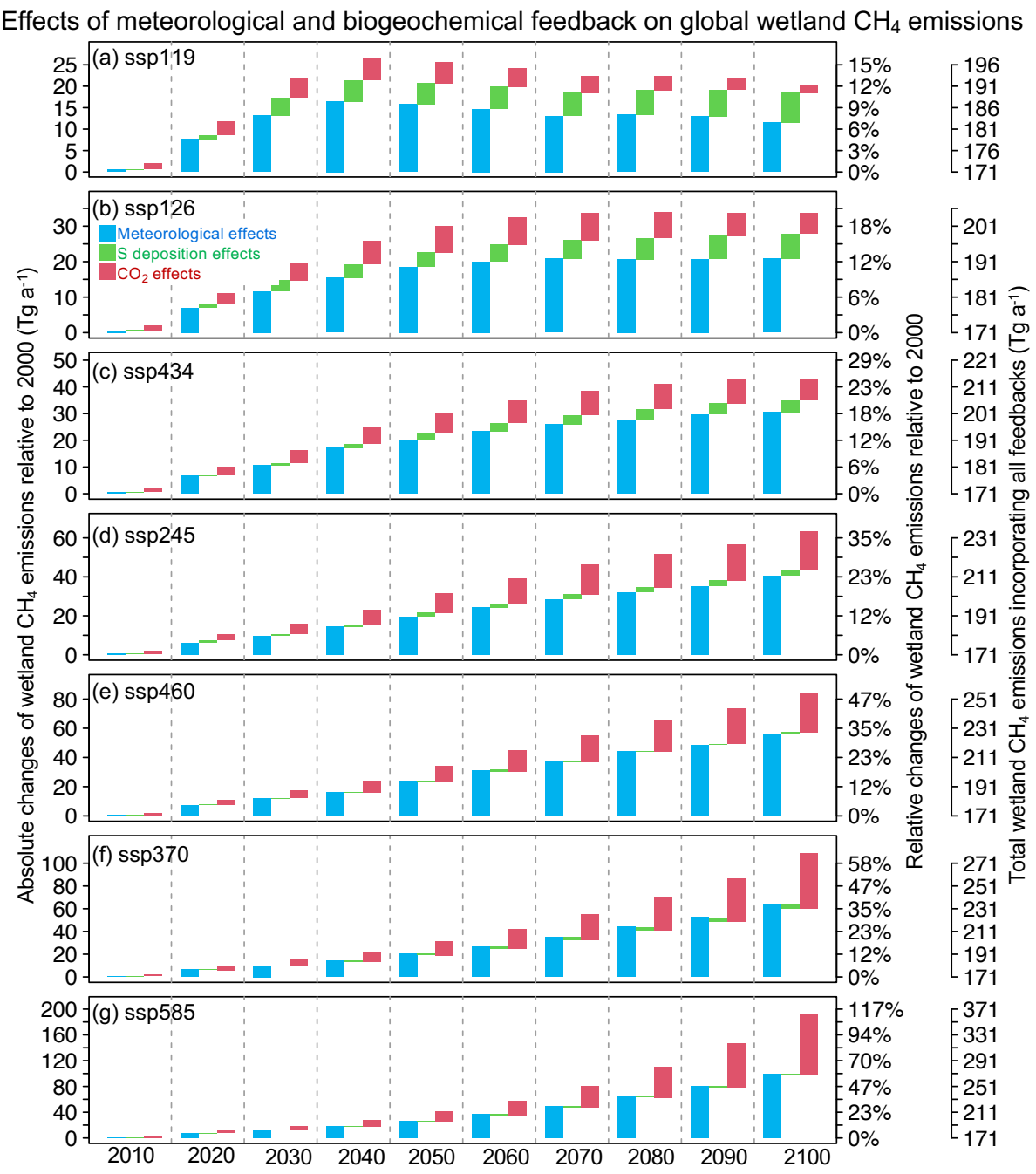


Fig. S13. **Wetland methane emissions relative to the 2000 baseline (171 Tg a^{-1}) across all 7 climate scenarios**, with the contribution of each feedback pathway. Emission changes are presented as both absolute and relative variations from the 2000 baseline. The rightmost y-axis indicate the total wetland methane emissions, incorporating all feedback pathways.

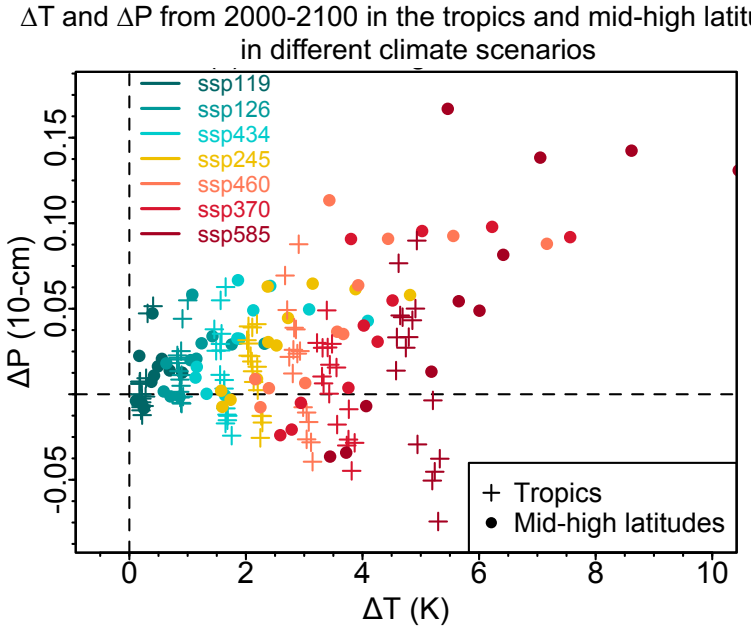


Fig. S14. The 2000-2100 changes of T and P in 7 climate scenarios for these latitudinal mean values in the tropics and mid-high latitudes. Tropics refer to the latitude band between 22.5°S and 22.5°N. Mid-high latitudes refer to regions north of 22.5°N and south of 22.5°S. The CMIP6 models used in the calculation here are listed in Table S2.

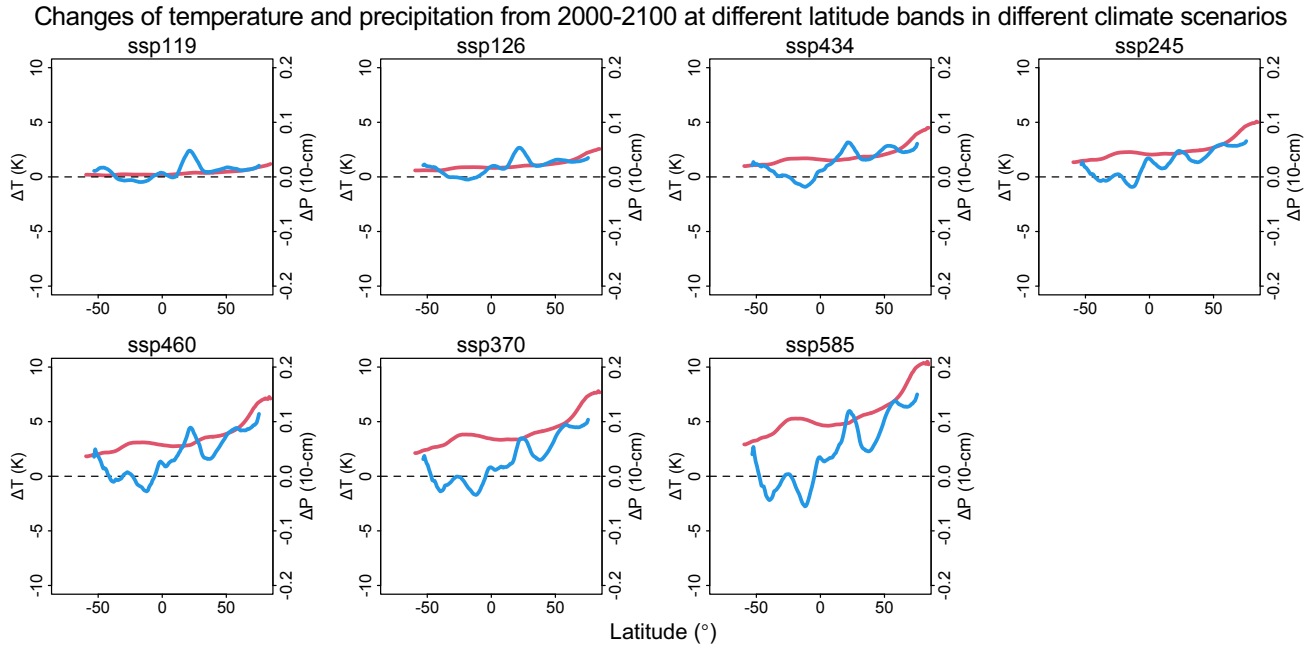


Fig. S15. Changes of temperature and precipitation from 2000-2100 at different latitude bands in ssp119, ssp126, ssp434, ssp245, ssp460, ssp370 and ssp585 scenarios. Each of the line denote the mean of all available models and realizations (see Table S2 for details).

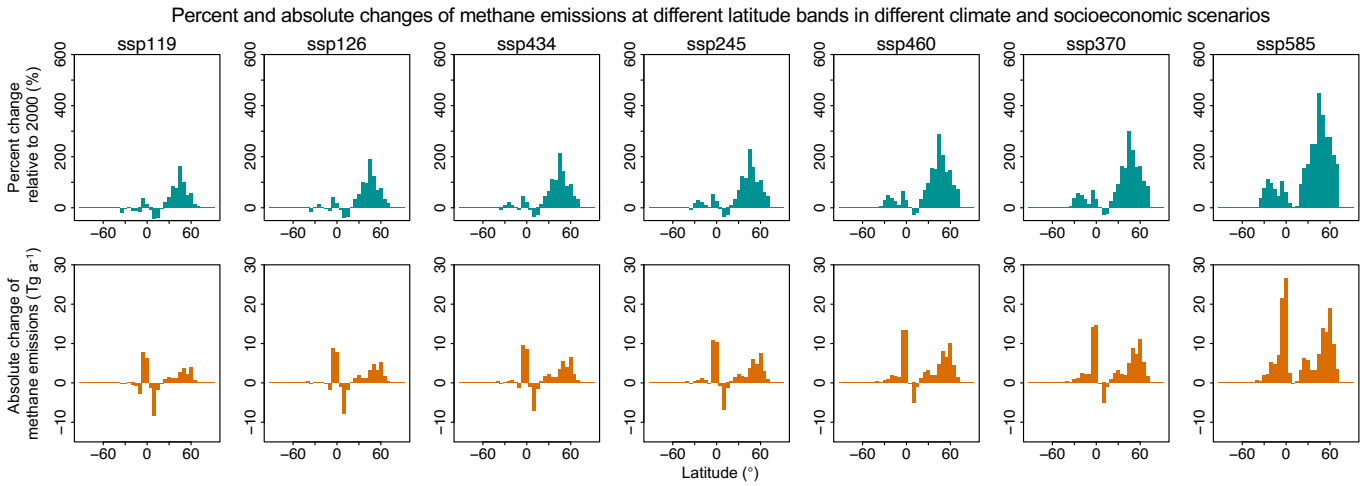


Fig. S16. Percent (top panel) and absolute changes (bottom panel) of wetland methane emissions from 2000-2100 in different latitude bands. Each bar represents the emissions for every 5° of latitude bands, averaged from all available experiments.

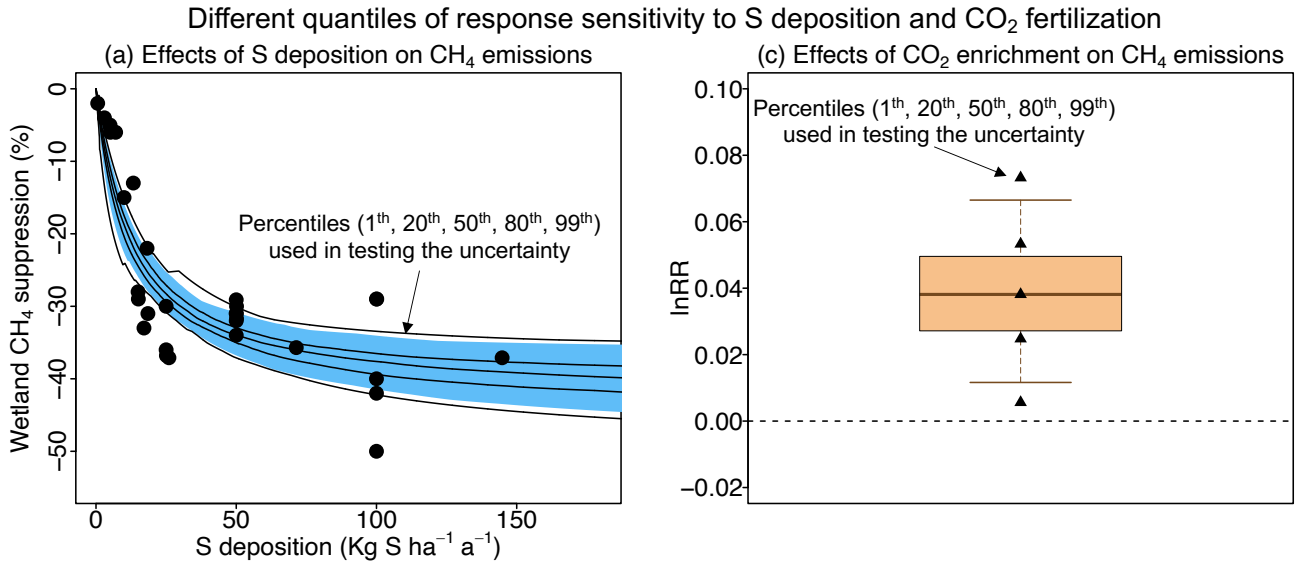


Fig. S17. **Different levels (from low to high) of response sensitivities of wetland methane emissions to (a) sulfate deposition and (b) CO_2 enrichment**. The lines in (a) and triangles in (b) denote the 1st, 20th, 50th, 80th, and 99th% quantiles of sensitivity from bootstrap resampling of field experiments (Data S2 and S3). More details can be found in Fig. 2.

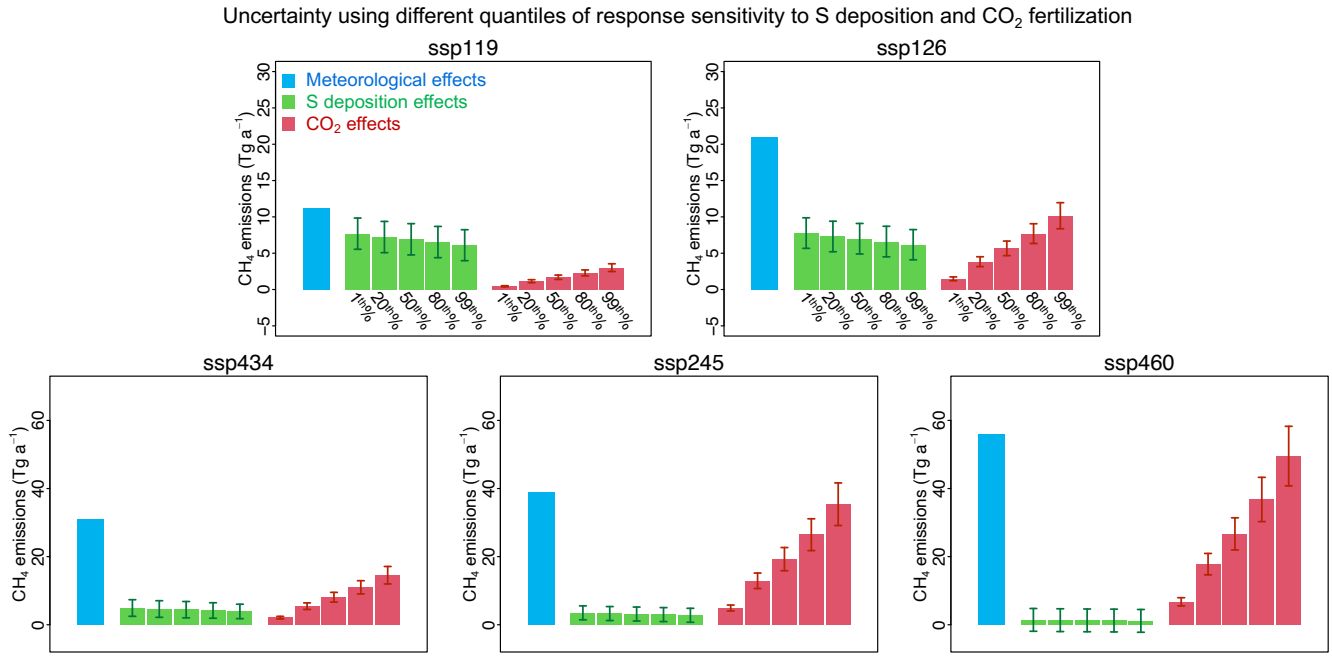


Fig. S18. The effects of meteorological and biogeochemical feedbacks (CO_2 fertilization, sulfate suppression) on wetland methane emissions from 2000 to 2100. For biogeochemical feedbacks, the changes are calculated using corresponding sensitivity levels at the 1st, 20th, 50th, 80th, and 99th percentiles (see Figure S15 for details).

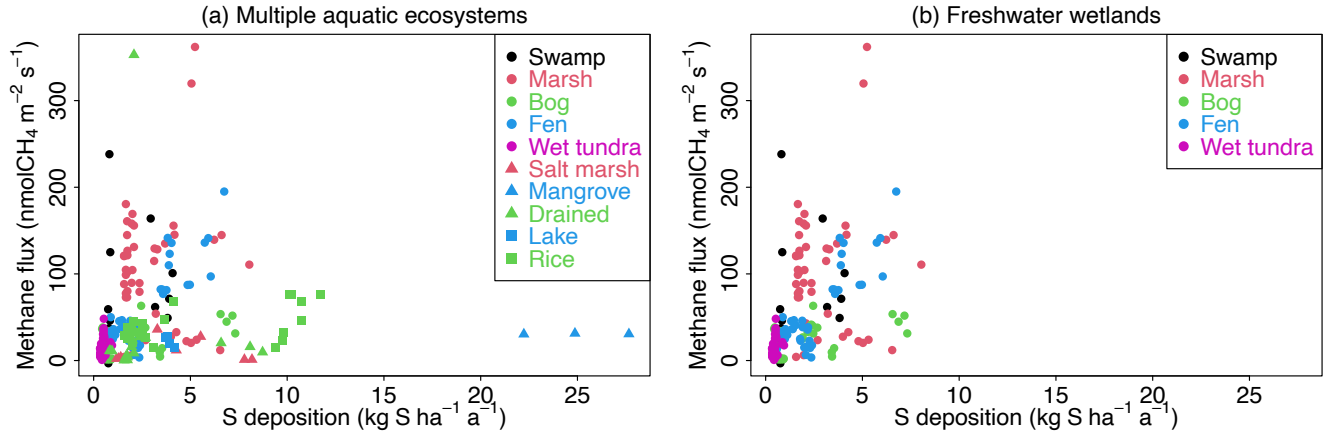


Fig. S19. Relationship of annual mean methane flux rates from site observations and sulfate deposition rates in (a) all aquatic ecosystems and (b) freshwater wetland only. Each point represents an observation in one particular year. Sulfate deposition rates are obtained from CovidMIP (https://doi.org/10.5194/gmd-14-3683-2021). We include all sites in FLUXNET-CH4, supplemented with a few sites from AmeriFlux (US-Cms, US-MBP and US-Sag, https://ameriflux.lbl.gov/) and EuroFlux (CZ-wet and DE-SfN, http://www.europe-fluxdata.eu/) with some of these observations dating back to the 2000s.

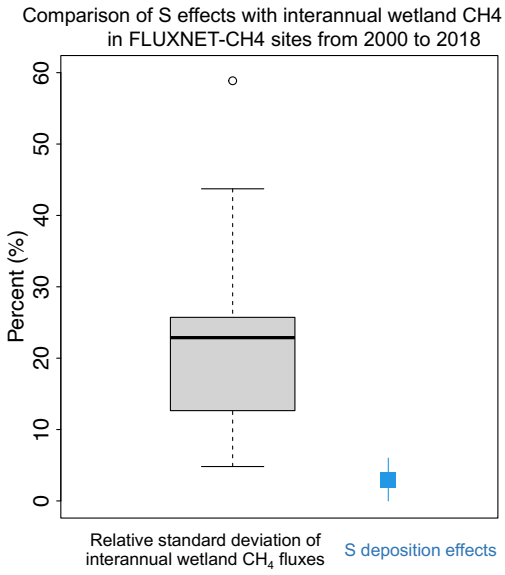


Fig. S20. **Comparison of sulfate deposition effects from 2000 to 2018 with the standard deviation of interannual wetland methane fluxes in FLUXNET-CH4 sites,** both expressed as relative changes to the mean methane fluxes. The effects of sulfate deposition on wetland methane fluxes are calculated by applying the empirical suppressive effects from field measurements (Fig. 2a) to atmospheric sulfate deposition rates in CovidMIP (https://doi.org/10.5194/gmd-14-3683-2021).

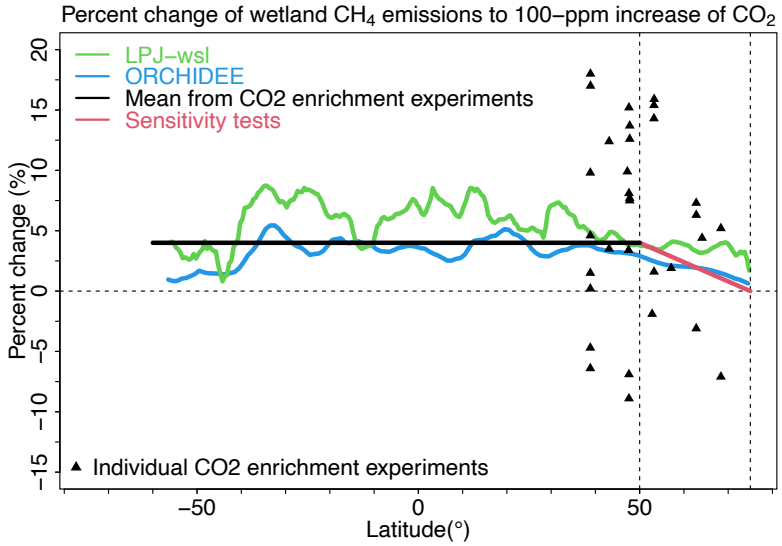


Fig. S21. **Percent change of wetland methane fluxes to a 100-pm increase of CO_2 concentrations in two land surface models (LPJ-wsl(*10*, *19*), ORCHIDEE(*71*)), with comparison to individual CO_2 enrichment experiment that are collected from previous literature and used in this study (Data S3)**. The red line denotes the sensitivity experiment we conducted to account for decreasing response sensitivity at high latitudes (north of 50°N), and the influence on wetland methane emissions can be found in Fig. 4. See more details in Methods.

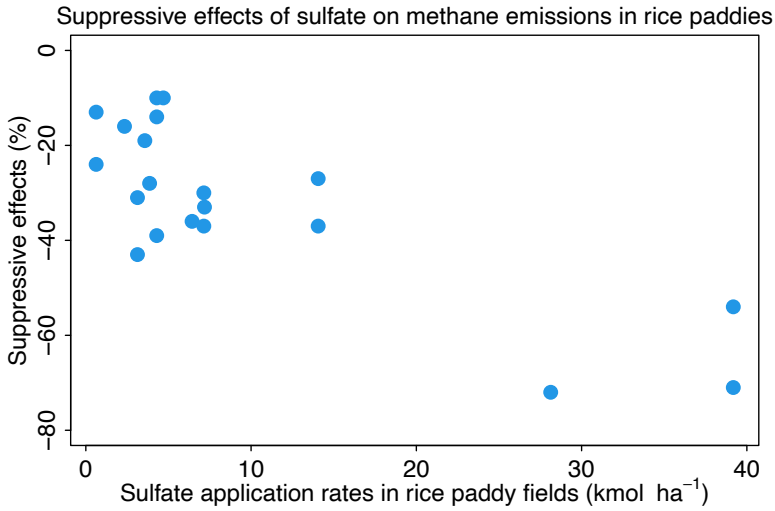


Fig. S22. **Relative changes of methane emissions in rice paddies after different sulfate application rates collected from field experiments**. This figure uses the data from Denier et al. (*73*) and additional measurements from Gauci et al.(*74*).

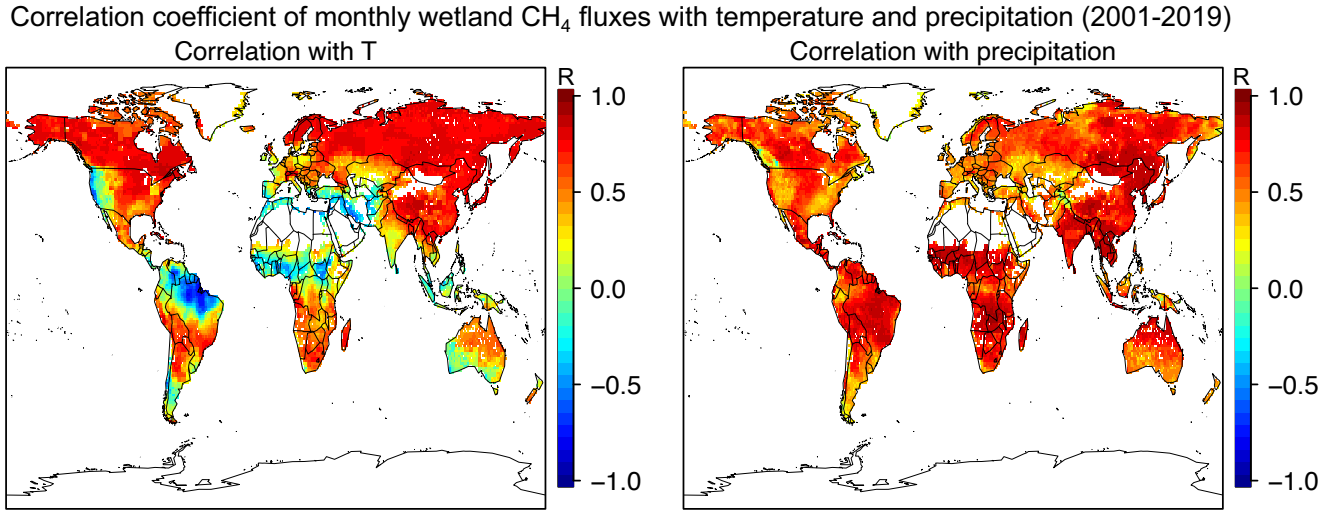


Fig. S23. **Correlations of monthly wetland methane fluxes with local temperature and precipitation**. Here, we calculate the correlation coefficient for every methane emission inventory (31 bottom-up and 8 top-down inventories), and the averaged values are shown here.

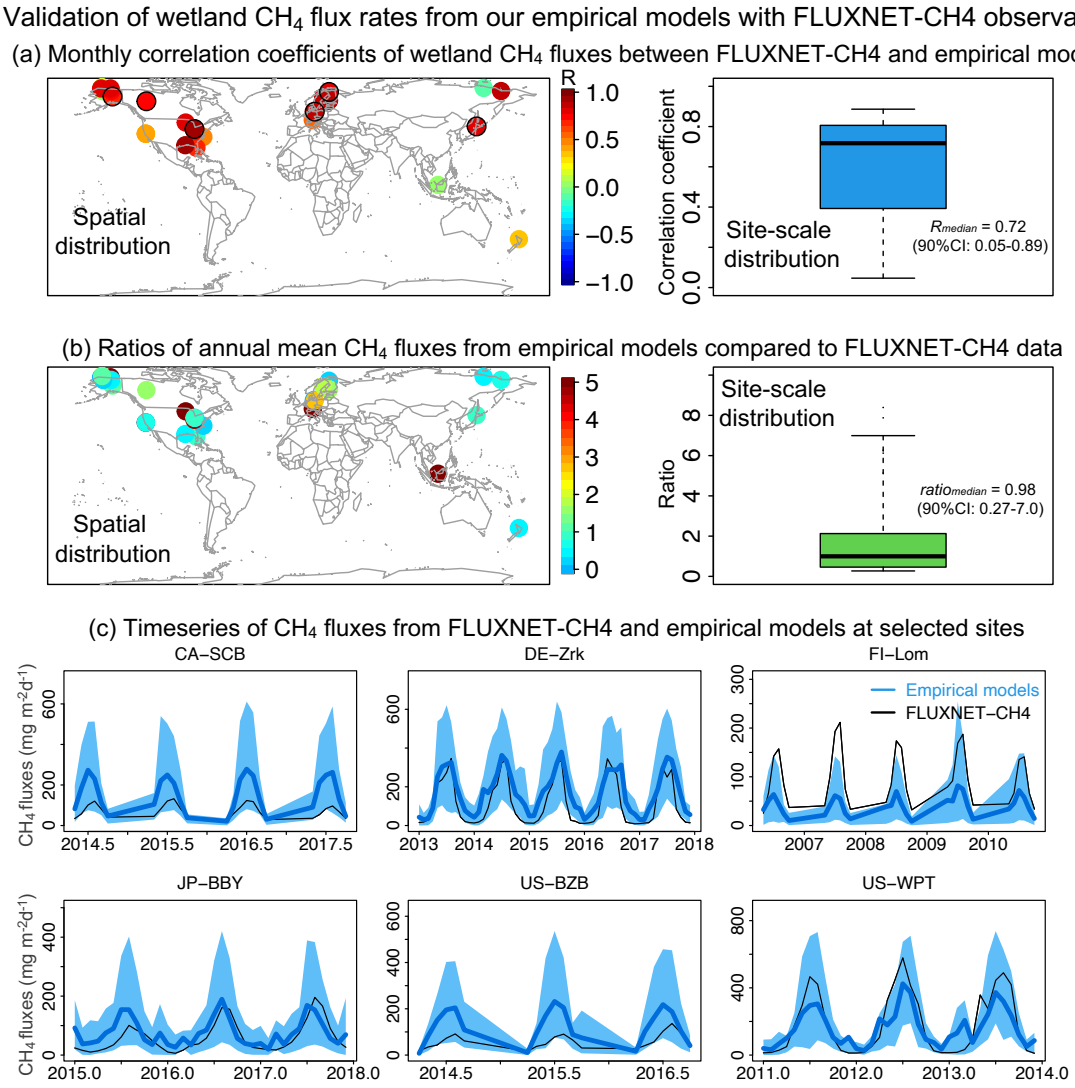


Fig. S24. Verification of methane fluxes from empirical models using FLUXNET-CH4 data. (a) Temporal correlation coefficients of wetland fluxes on a monthly scale, calculated for sites with at least 12 months of observations. The boxplot illustrates the distribution of correlation coefficients from all sites. (b) Ratios of annual mean CH_4 fluxes from empirical models compared to those from FLUXNET-CH4 sites. (c) Monthly CH_4 fluxes from our empirical models and FLUXNET-CH4 sites for 6 representative sites. Black circles in Panel (a) denote the locations of these 6 sites. Please note that our empirical models are trained at ~100 km resolution.

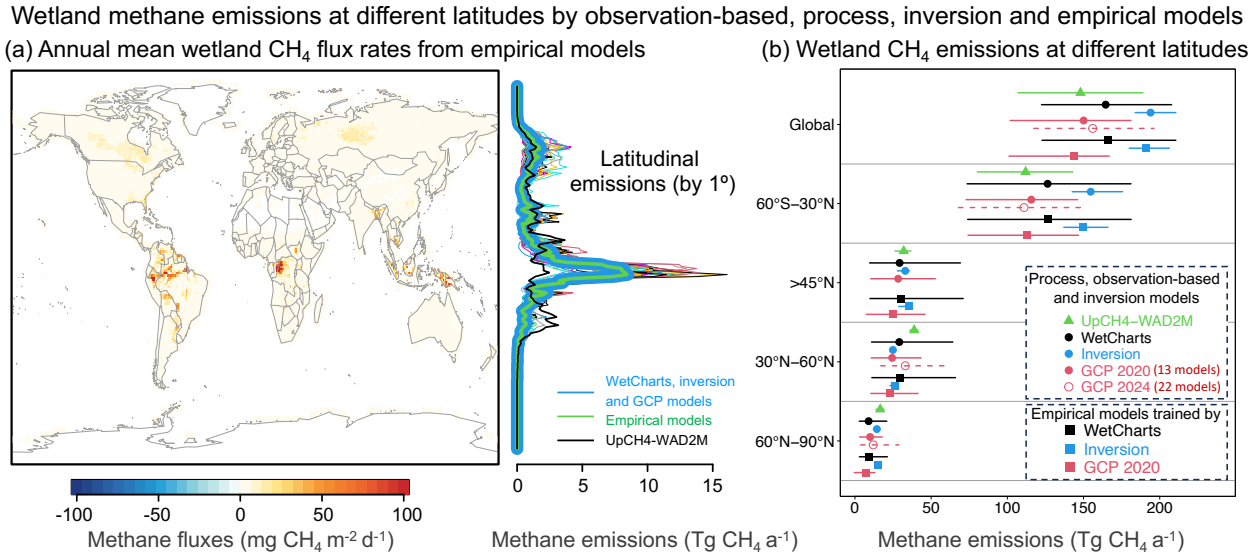


Fig. S25. **Comparison of annual wetland methane emissions** globally and by latitudes across different datasets. (a) Wetland methane fluxes from empirical models at a 1°×1° horizontal resolution. The right panel shows the latitudinal emissions from empirical models, WetCharts, atmospheric inversions, GCP models (Table S1), and UPCH4(*83*) (upscaled from FLUXNET-CH4 using the wetland area WAD2M(*82*)), all integrated at 1° intervals. (b) Comparison of wetland CH_4 emissions from different datasets, integrated across different latitude bands. The comparison also includes 22 models that participated in the latest Global Carbon Project for the methane budget (*5*). According to McNico et al. (*83*), the UpCH4 product is subject to high uncertainty in (sub)tropical regions due to observation scarcity (7 sites), and is more suitable for comparison in non-tropical wetlands.

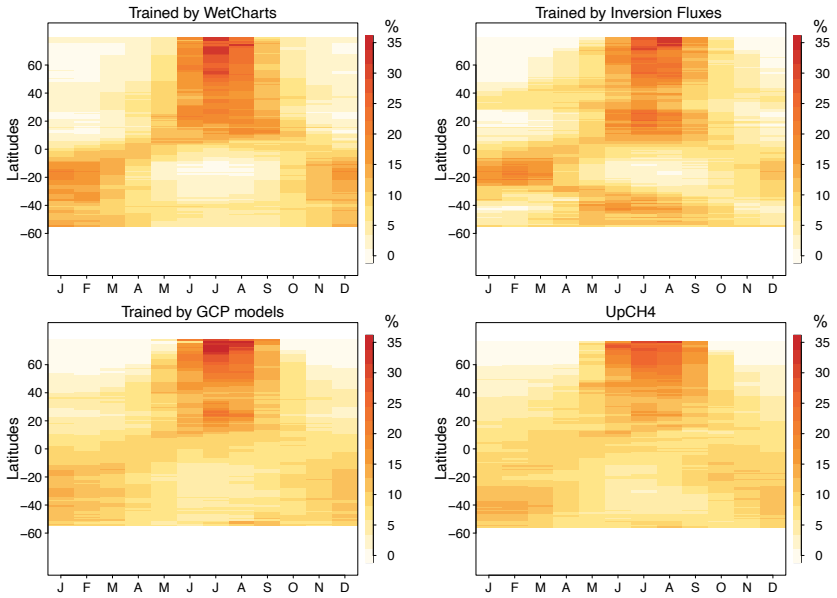


Fig. S26. **Comparison of percent emissions in different months from wetlands at different latitude bands**. The numbers are calculated among empirical models trained by WetCharts, atmospheric inversion, and GCP models (Table S1), which are compared with these in UpCH4.

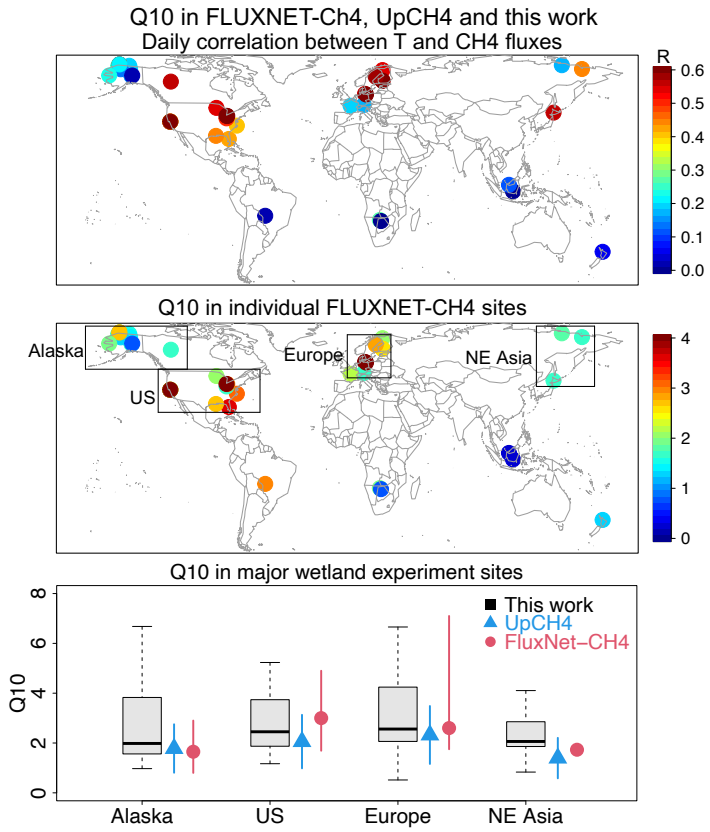


Fig. S27. **Comparison of temperature dependence (Q10) among UpCH4, FLUXNET-CH4 and models used in this work.** (a) The correlation coefficient of wetland methane fluxes from the empirical models developed in this work and surface air temperature. (b) Q10 in different FLUXNET-CH4 sites. (c) Q10 among UpCH4, FLUXNET-CH_4 and this work in four boreal wetland regions.

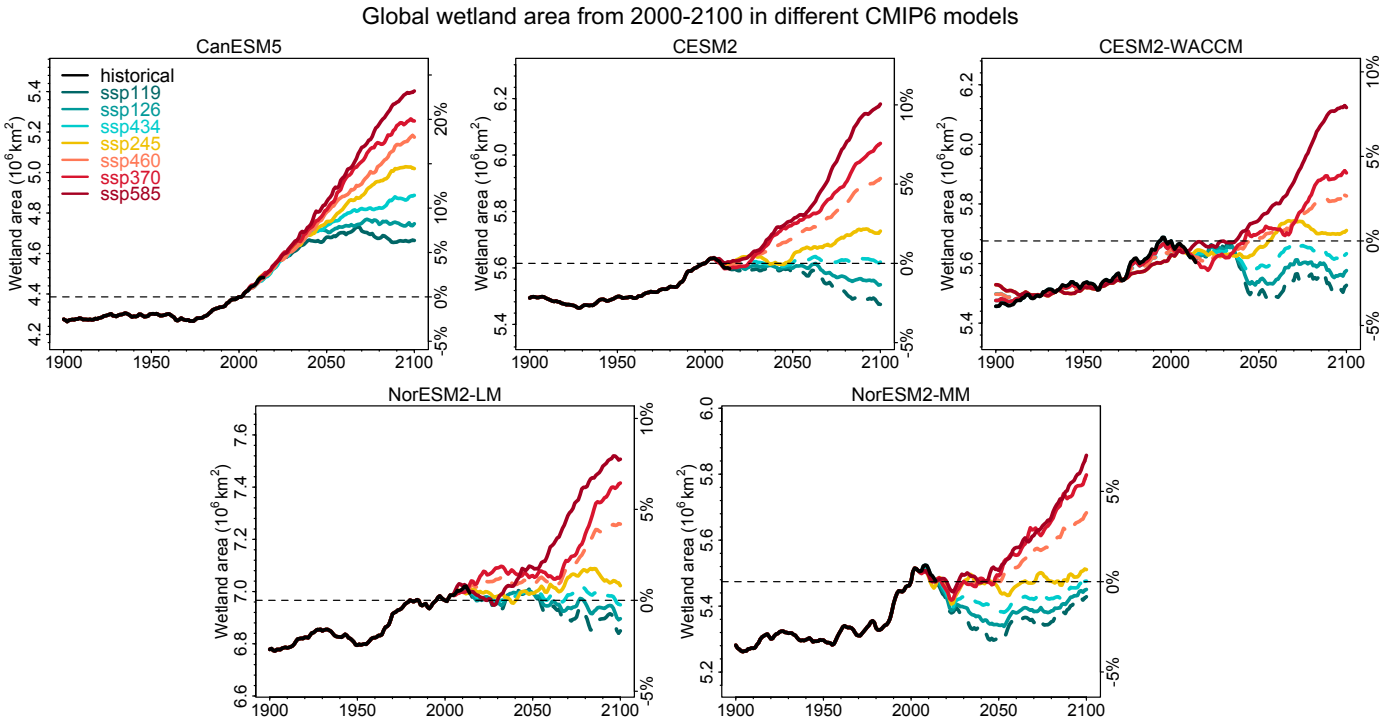


Fig. S28. **Global wetland area in different CMIP6 models.** The dashed line denotes the emissions in the year 2000. Among these models, only CanESM5 provides outputs for all the historical and 7 future climate scenarios. Thus, we estimate the wetland area of the missing scenarios using a simple linear interpolation based on those of nearest radiative forcing.

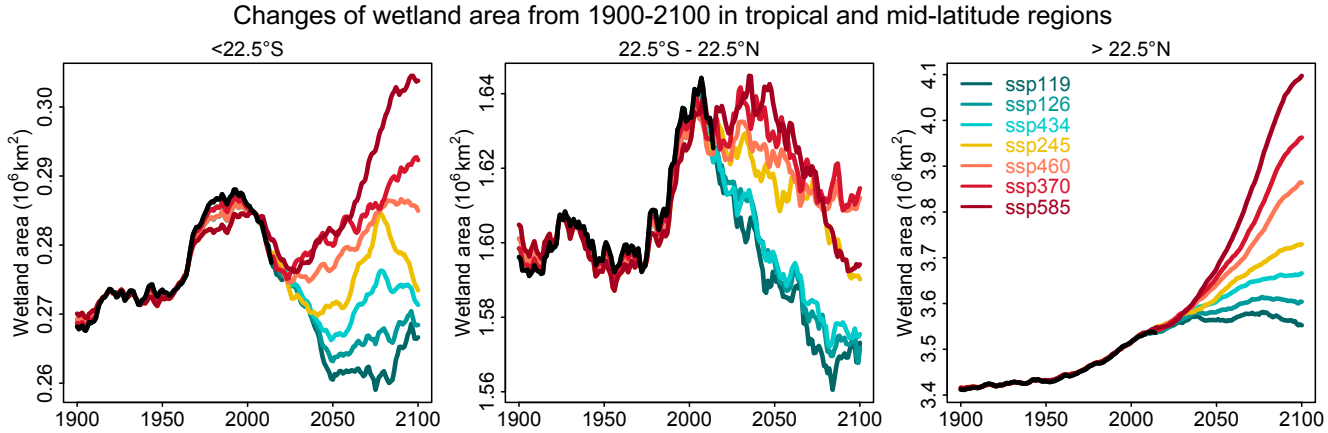


Fig. S29. **Timeseries of global wetland area from 1900-2100 in tropical and mid-latitude regions**, averaged from outputs of 5 CMIP6 models.

Table S1. Bottom-up and top-down inventories to constrain meteorological sensitivities (N=39) in this work.

Methods	Model #	Resolution	Timeframe	Emissions (Tg a^{-1})	Inputs	References
WetCharts v1.3.1	Model 1	0.5°×0.5°	2000-2019	124.2		Bloom et al.(*49*)
	Model 2			123.7		
	Model 3			122.0		
	Model 4			121.7		
	Model 5			120.9		
	Model 6			120.7		
	Model 7			165.6		
	Model 8			164.9		
	Model 9			162.7		
	Model 10			162.2		
	Model 11			161.2		
	Model 12			160.9		
	Model 13			207.0		
	Model 14			206.2		
	Model 15			203.3		
	Model 16			202.8		
	Model 17			201.5		
	Model 18			201.1		
Land process models participating in the GCP project	CLASS-CTEM	0.5°×0.5°	2008-2017	180.7		Saunois et al. (*3*)
	DLEM			150.3		
	ELM			164.9		
	JSBACH			129.7		
	JULES			182.5		
	LPJ-GUESS			166.3		
	LPJ-MPI			162.0		
	LPJ-WSL			145.1		
	LPX			138.6		
	ORCHIDEE			142.6		
	TEM-MDM			106.5		
	TRIPLEX-GHG			102.4		
	VISIT			163.2		
Top-down	CAMS_v11r1	3°×2°	2000-2015	185.0	surface air-sample measurements	https://www.ecmwf.int/en/forecasts/dataset/cams-greenhouse-gas-ghg-flux-inversions
	CAMS_v16r1	3°×2°	2000-2016	188.7	surface air-sample measurements	
	CAMS_v16r1s	3°×2°	2000-2016	187.8	surface air-sample and satellite measurements	
	CAMS_v16r2	3°×2°	2000-2016	189.6	surface air-sample measurements	
	CAMS_v17r1	3°×2°	2000-2017	191.6	surface air-sample measurements	
	CAMS_v17r1s	3°×2°	2000-2017	190.9	surface air-sample and satellite measurements	
	MACC-III_v10-S1NOAA	6°×4°	2000-2012	204.1	NOAA surface observations	
	MACC-III_v10-S1SCIA	6°×4°	2000-2012	205.4	NOAA surface observations and the XCH4 satellite retrievals from SCIAMACHY	

Table S2. Projection of meteorology in different scenarios by CMIP6 models*.

Scenarios	# of models	Model names	# of realizations
historical	30	ACCESS-CM2, ACCESS-ESM1-5, AWI-CM-1-1-MR, BCC-CSM2-MR, BCC-ESM1, CAMS-CSM1-0, CanESM5, CanESM5-CanOE, CAS-ESM2-0, CESM2, CMCC-CM2-HR4, CMCC-CM2-SR5, CMCC-ESM2, CNRM-CM6-1, CNRM-CM6-1-HR, CNRM-ESM2-1, E3SM-1-0, E3SM-1-1-ECA, EC-Earth3, FGOALS-f3-L, FGOALS-g3, FIO-ESM-2-0, GFDL-ESM4, GISS-E2-1-G, GISS-E2-1-H, IITM-ESM, IPSL-CM6A-LR, MPI-ESM1-2-HR, NESM3, TaiESM1	83
ssp119	9	CAMS-CSM1-0, CanESM5, CNRM-ESM2-1, EC-Earth3, FGOALS-g3, GFDL-ESM4, GISS-E2-1-H, IPSL-CM6A-LR, MPI-ESM1-2-LR	31
ssp126	30	ACCESS-CM2, ACCESS-ESM1-5, AWI-CM-1-1-MR, BCC-CSM2-MR, CAMS-CSM1-0, CanESM5, CanESM5-CanOE, CAS-ESM2-0, CESM2, CMCC-CM2-SR5, CMCC-ESM2, CNRM-CM6-1, CNRM-CM6-1-HR, CNRM-ESM2-1, EC-Earth3, FGOALS-f3-L, FGOALS-g3, GFDL-ESM4, GISS-E2-1-H, IITM-ESM, INM-CM4-8, INM-CM5-0, IPSL-CM5A2-INCA, IPSL-CM6A-LR, KACE-1-0-G, MPI-ESM1-2-HR, NESM3, NorESM2-LM, NorESM2-MM, TaiESM1	64
ssp434	6	CanESM5, CNRM-ESM2-1, EC-Earth3, FGOALS-g3, GISS-E2-1-H, IPSL-CM6A-LR	20
ssp245	24	ACCESS-CM2, ACCESS-ESM1-5, AWI-CM-1-1-MR, BCC-CSM2-MR, CAMS-CSM1-0, CanESM5, CanESM5-CanOE, CAS-ESM2-0, CESM2, CMCC-CM2-SR5, CMCC-ESM2, CNRM-CM6-1, CNRM-CM6-1-HR, CNRM-ESM2-1, E3SM-1-1, EC-Earth3, FGOALS-f3-L, FGOALS-g3, GFDL-ESM4, IITM-ESM, INM-CM4-8, MPI-ESM1-2-HR, NorESM2-MM, TaiESM1	64
ssp460	6	CanESM5, CNRM-ESM2-1, EC-Earth3, FGOALS-g3, GISS-E2-1-H, IPSL-CM6A-LR	23
ssp370	25	ACCESS-CM2, ACCESS-ESM1-5, AWI-CM-1-1-MR, BCC-CSM2-MR, BCC-ESM1, CAMS-CSM1-0, CanESM5, CanESM5-CanOE, CAS-ESM2-0, CESM2, CMCC-CM2-SR5, CMCC-ESM2, CNRM-CM6-1, CNRM-CM6-1-HR, CNRM-ESM2-1, EC-Earth3, FGOALS-f3-L, FGOALS-g3, GFDL-ESM4, GISS-E2-2-G, IITM-ESM, INM-CM4-8, MPI-ESM1-2-HR, NorESM2-LM, TaiESM1	73
ssp585	28	ACCESS-CM2, ACCESS-ESM1-5, AWI-CM-1-1-MR, BCC-CSM2-MR, CAMS-CSM1-0, CanESM5, CanESM5-CanOE, CAS-ESM2-0, CMCC-CM2-SR5, CMCC-ESM2, CNRM-CM6-1, CNRM-CM6-1-HR, CNRM-ESM2-1, E3SM-1-0, E3SM-1-1, E3SM-1-1-ECA, EC-Earth3, FGOALS-f3-L, FGOALS-g3, GFDL-ESM4, GISS-E2-1-H, IITM-ESM, IPSL-CM6A-LR, MPI-ESM1-2-HR, NESM3, NorESM2-LM, NorESM2-MM, TaiESM1	65
All	39	ACCESS-CM2, ACCESS-ESM1-5, AWI-CM-1-1-MR, BCC-CSM2-MR, BCC-ESM1, CAMS-CSM1-0, CanESM5-CanOE, CanESM5, CAS-ESM2-0, CESM2, CMCC-CM2-HR4, CMCC-CM2-SR5, CMCC-ESM2, CNRM-CM6-1-HR, CNRM-CM6-1, CNRM-ESM2-1, E3SM-1-0, E3SM-1-1-ECA, EC-Earth3, FGOALS-f3-L, FGOALS-g3, FIO-ESM-2-0, GFDL-ESM4, GISS-E2-1-G, GISS-E2-1-H, IITM-ESM, IPSL-CM6A-LR, MPI-ESM1-2-HR, NESM3, TaiESM1, MPI-ESM1-2-LR, INM-CM4-8, INM-CM5-0, IPSL-CM5A2-INCA, KACE-1-0-G, NorESM2-LM, NorESM2-MM, E3SM-1-1, GISS-E2-2-G	423

*For each model and each climate scenario, we include up to 5 realizations (e.g. r1i1p1f1, r2i1p1f1) to fully consider the spread of climate sensitivity due to randomization in model setups and spin-ups. For Tier 1 scenarios (historical, ssp126, ssp245, ssp37, and ssp585), at least 24 models and >60 realizations are used in the analysis. For Tier 2 scenarios (ssp119, ssp434, ssp460), fewer but still a sufficient number of models (6-9) and realizations (>20) are available for evaluation.

Table S3. Projection of sulfate deposition in different scenarios by AerChemMIP models.

Model	Available scenarios
CanESM5	historical, ssp119, ssp126, ssp245, ssp370, ssp434, ssp460, ssp585
GFDL-ESM4	historical, ssp119, ssp126, ssp245, ssp370, ssp585
MIROC-ES2L	historical, ssp119, ssp245, ssp370, ssp585
MRI-ESM2-0	historical, ssp119, ssp126, ssp245, ssp370, ssp434, ssp460, ssp585

Table S4. Meteorological and biogeochemical feedback on 2000-2100 wetland methane emissions.

Scenarios	Met effects ($Tg\ a^{-1}$)	Biogeochemical effects ($Tg\ a^{-1}$)			Total effect ($Tg\ a^{-1}$)	Ratio of biogeochemical to meteorological feedback effects			
		S effects	CO_2 effects	S+CO_2 effect		S/meteorology	CO_2/meteorology	(S+CO_2)/meteorology	(S+CO_2)/Total
ssp119	11.2	6.9	1.7 (1.7)	8.6	19.9	61.4%	15.2%	76.7%	43.5%
ssp126	21.0	7.0	5.7 (5.0)	12.7	33.7	33.2%	27.3%	60.5%	37.7%
ssp434	31.1	4.4	8.2 (7.0)	12.6	43.6	14.1%	26.3%	40.4%	28.8%
ssp245	39.0	3.1	19.6 (16.5)	22.7	61.6	8.0%	50.2%	58.2%	36.8%
ssp460	56.2	1.2	27.1 (22.8)	28.4	84.5	2.2%	48.3%	50.5%	33.5%
ssp370	63.6	-4.2	47.9 (40.2)	43.6	107.2	-6.6%	75.3%	68.7%	40.7%
ssp585	99.6	0.1	91.9 (76.9)	91.9	191.4	0.1%	92.3%	92.3%	48%

†The number in parathesis denote the effects of CO_2 fertilization on wetland methane emissions after excluding C4-plants from calculation.

Table S5. Comparison of projected wetland methane emissions with previous studies.

Reference	Parameterization of biogeochemical feedback		Method details		Historical emissions (Tg a^{-1})	ΔCH4 emissions from 2000-2100 (Tg a^{-1})						
	CO_2 effects‡	S effects	Method (including land surface model names if used)	Description†		SSP119	SSP126	SSP434	SSP245	SSP460	SSP370	SSP585
							B1		A1B			A2
							RCP2.6		RCP4.5	RCP6.0		RCP8.5
This study	yes, type 1	yes	Data-driven	31 LSM + 8 INV, 7 scenarios	**174**	**20**	**34**	**44**	**62**	**85**	**107**	**191**
Zhang et al.(*10*)	yes, type 2	no	LPJ-wsl	1 LSM, 4 scenarios	175		36		72	93		163
Koffi et al.(*18*)	no	no	Data-driven	17 LSM + 11 INV, 4 scenarios	175		14		33	41		90
Gedney et al. (*20*)	yes, type 2	no	JULES-CS, JULES-NPP	1 LSM, 4 scenarios	173		4.9-36.0		16.2-92.2			40.8-269
Zhang et al.(*19*)	yes, type 2	no	LPJ-wsl	1 LSM, 4 scenarios	172		49.6		83	100		166
Stocker et al.(*24*)	yes, type 2	no	LPX-Bern 1.0	1 LSM, 2 scenarios	221		7.0-24.0					82-122
Ringeval et al.(*92*)	yes, type 2	no	ORCHIDEE-WET	1 LSM, 1 scenario	251							173-321
Eliseev et al.(*21*)	no	no	IAP RAS CM + CH_4 parametrization	1 LSM, 3 scenarios	133-139		31-34		44-46			58-60
Volodin et al.(*35*)	yes, type 2	no	INM + LSM	1 LSM, 1 scenario	240							100
Shindell et al.(*22*)	yes, type 2	no	GISS Model II	1 LSM, 1 scenario	156							121
Gedney et al.(*23*)	yes, type 2	no	MOSES-LSH	1 LSM, 1 scenario	298							255

‡Type 1 refers statistical parameterization of CO_2 fertilization effects directly constrained by experimental data. Type 2 refers to representation of CO_2 effects through biosphere feedback (e.g., NPP and soil carbon).

†LSM refers to land surface models. INV refers to using inventory from atmospheric inversions.

Table S6. Projected changes of wetland CH_4 emissions in ssp119 and ssp126 scenarios, compared to major global CH_4 sources and mitigation targets.

References	CH_4 mitigation potential or sources ($Tg\ a^{-1}$)	Timeframe or emission years
Wetland methane emissions in ssp119 and ssp126 scenarios		
ΔEmissions in ssp119	20	2000-2100
	14	2020-2050
	10	2020-2030
ΔEmissions in ssp126	33	2000-2100
	19	2020-2050
	9	2020-2030
Major global CH_4 sources		
Global ocean emissions	9	Present-day
Global aquaculture emissions	6-14	Present-day
Global source - sink net budget from an ensemble of atmospheric inversion studies (*3*)	13 (0-49)	2008-2017
Global source - sink net budget from atmospheric methane growth* (*93*)	14 ± 12	2000-2019
The US oil-gas emissions (*67*)	13 ± 2	2018
China's coal emissions	19	2019
Global coal emissions - UNFCCC (*68*)	33	2019
Global oil-gas emissions - UNFCCC (*68*)	48	2019
Mitigation targets from different estimates		
Global agricultural mitigation target toward the 1.5°C goal (*94*)	55 (30-80)	2030
Global energy mitigation target toward the 1.5°C goal (*94*)	125 (100-150)	2030
Global methane pledge (reducing methane emissions by 30%)(*69*)	108	2030
Changes of anthropogenic methane emissions in the ssp119 scenario(*38*)	100	2020-2030
	180	2020-2050
Changes of anthropogenic methane emissions in the ssp126 scenario(*38*)	60	2020-2030
	130	2020-2050

* The 20-year mean atmospheric methane growth rates are 4.9 ± 4.3 ppb a^{-1} (https://gml.noaa.gov/ccgg/trends_ch4/). We obtain the growth of atmospheric methane emissions based on the conversion factor of 2.75 Tg CH_4 ppb^{-1} given by Prather et al. (*93*).

Data S1

Wetland methane emissions collected from 135 estimates using bottom-up and top-down approaches. See Extended_Data_S1.xlsx for details.

Data S2

Suppressive effects of sulfate deposition on wetland methane emissions from 30 controlled experiments. See Extended_Data_S2.xlsx for details.

Data S3

Effects of CO_2 enrichment on wetland CH_4 emissions from 118 experiments in 34 individual sites. See Extended_Data_S3.xlsx for details.

REFERENCES AND NOTES

1. V. Naik, S. Szopa, B. Adhikary, P. Artaxo, T. Berntsen, W. D. Collins, S. Fuzzi, L. Gallardo, A. Kiendler Scharr, Z. Klimont, H. Liao, N. Unger, P. Zanis, "Short-lived climate forcers" in *Climate Change 2021: The Physical Science Basis. Contribution of Working Group I to the Sixth Assessment Report of the Intergovernmental Panel on Climate Change*, V. Masson-Delmotte, P. Zhai, A. Pirani, S. L. Connors, C. Péan, S. Berger, N. Caud, Y. Chen, L. Goldfarb, M. I. Gomis, M. Huang, K. Leitzell, E. Lonnoy, J. B. R. Matthews, T. K. Maycock, T. Waterfield, O. Yelekçi, R. Yu and B. Zhou, Eds. (Cambridge Univ. Press, 2021), pp. 817–922.

2. S. Kirschke, P. Bousquet, P. Ciais, M. Saunois, J. G. Canadell, E. J. Dlugokencky, P. Bergamaschi, D. Bergmann, D. R. Blake, L. Bruhwiler, P. Cameron-Smith, S. Castaldi, F. Chevallier, L. Feng, A. Fraser, M. Heimann, E. L. Hodson, S. Houweling, B. Josse, P. J. Fraser, P. B. Krummel, J.-F. Lamarque, R. L. Langenfelds, C. Le Quéré, V. Naik, S. O'Doherty, P. I. Palmer, I. Pison, D. Plummer, B. Poulter, R. G. Prinn, M. Rigby, B. Ringeval, M. Santini, M. Schmidt, D. T. Shindell, I. J. Simpson, R. Spahni, L. P. Steele, S. A. Strode, K. Sudo, S. Szopa, G. R. van der Werf, A. Voulgarakis, M. van Weele, R. F. Weiss, J. E. Williams, G. Zeng, Three decades of global methane sources and sinks. *Nat. Geosci.* **6**, 813–823 (2013).

3. M. Saunois, A. R. Stavert, B. Poulter, P. Bousquet, J. G. Canadell, R. B. Jackson, P. A. Raymond, E. J. Dlugokencky, S. Houweling, P. K. Patra, P. Ciais, V. K. Arora, D. Bastviken, P. Bergamaschi, D. R. Blake, G. Brailsford, L. Bruhwiler, K. M. Carlson, M. Carrol, S. Castaldi, N. Chandra, C. Crevoisier, P. M. Crill, K. Covey, C. L. Curry, G. Etiope, C. Frankenberg, N. Gedney, M. I. Hegglin, L. Höglund-Isaksson, G. Hugelius, M. Ishizawa, A. Ito, G. Janssens-Maenhout, K. M. Jensen, F. Joos, T. Kleinen, P. B. Krummel, R. L. Langenfelds, G. G. Laruelle, L. Liu, T. Machida, S. Maksyutov, K. C. McDonald, J. McNorton, P. A. Miller, J. R. Melton, I. Morino, J. Müller, F. Murguia-Flores, V. Naik, Y. Niwa, S. Noce, S. O'Doherty, R. J. Parker, C. Peng, S. Peng, G. P. Peters, C. Prigent, R. Prinn, M. Ramonet, P. Regnier, W. J. Riley, J. A. Rosentreter, A. Segers, I. J. Simpson, H. Shi, S. J. Smith, L. P. Steele, B. F. Thornton, H. Tian, Y. Tohjima, F. N. Tubiello, A. Tsuruta, N. Viovy, A. Voulgarakis, T. S. Weber, M. van Weele, G. R. van der Werf, R. F. Weiss, D. Worthy, D. Wunch, Y. Yin, Y. Yoshida, W. Zhang, Z. Zhang, Y. Zhao, B. Zheng, Q. Zhu, Q. Zhu, Q. Zhuang, The global methane budget 2000–2017. *Earth Syst. Sci. Data* **12**, 1561–1623 (2020).

4. S. Basu, X. Lan, E. Dlugokencky, S. Michel, S. Schwietzke, J. B. Miller, L. Bruhwiler, Y. Oh, P. P. Tans, F. Apadula, L. V. Gatti, A. Jordan, J. Necki, M. Sasakawa, S. Morimoto, T. Di Iorio, H. Lee, J. Arduini, G. Manca, Estimating emissions of methane consistent with atmospheric measurements of methane and δ^{13}C of methane. *Atmos. Chem. Phys.* **22**, 15351–15377 (2022).

5. M. Saunois, A. Martinez, B. Poulter, Z. Zhang, P. Raymond, P. Regnier, J. G. Canadell, R. B. Jackson, P. K. Patra, P. Bousquet, P. Ciais, E. J. Dlugokencky, X. Lan, G. H. Allen, D. Bastviken, D. J. Beerling, D. A. Belikov, D. R. Blake, S. Castaldi, M. Crippa, B. R. Deemer, F. Dennison, G. Etiope, N. Gedney, L. Höglund-Isaksson, M. A. Holgerson, P. O. Hopcroft, G. Hugelius, A. Ito, A. K. Jain, R. Janardanan, M. S. Johnson, T. Kleinen, P. Krummel, R. Lauerwald, T. Li, X. Liu, K. C. McDonald, J. R. Melton, J. Mühle, J. Müller, F. Murguia-Flores, Y. Niwa, S. Noce, S. Pan, R. J. Parker, C. Peng, M. Ramonet, W. J. Riley, G. Rocher-Ros, J. A. Rosentreter, M. Sasakawa, A. Segers, S. J. Smith, E. H. Stanley, J. Thanwerdas, H. Tian, A. Tsuruta, F. N. Tubiello, T. S. Weber, G. Van Der Werf, D. E. Worthy, Y. Xi, Y. Yoshida, W. Zhang, B. Zheng, Q. Zhu, Q. Zhu, Q. Zhuang, Global methane budget 2000–2020. *Earth Syst. Sci. Data Discuss.* , (2024). https://doi.org/10.5194/essd-2024-115.

6. E. G. Nisbet, E. J. Dlugokencky, M. R. Manning, D. Lowry, R. E. Fisher, J. L. France, S. E. Michel, J. B. Miller, J. W. C. White, B. Vaughn, P. Bousquet, J. A. Pyle, N. J. Warwick, M. Cain, R. Brownlow, G. Zazzeri, M. Lanoisellé, A. C. Manning, E. Gloor, D. E. J. Worthy, E.-G. Brunke, C. Labuschagne, E. W. Wolff, A. L. Ganesan, Rising atmospheric methane: 2007-2014 Growth and isotopic shift: RISING METHANE 2007–2014. *Global Biogeochem. Cycles* **30**, 1356–1370 (2016).

7. E. G. Nisbet, M. R. Manning, E. J. Dlugokencky, R. E. Fisher, D. Lowry, S. E. Michel, C. L. Myhre, S. M. Platt, G. Allen, P. Bousquet, R. Brownlow, M. Cain, J. L. France, O. Hermansen, R. Hossaini, A. E. Jones, I. Levin, A. C. Manning, G. Myhre, J. A. Pyle, B. H. Vaughn, N. J. Warwick, J. W. C. White, Very strong atmospheric methane growth in the 4 years 2014–2017: Implications for the Paris agreement. *Global Biogeochem. Cycles* **33**, 318–342 (2019).

8. E. G. Nisbet, M. R. Manning, E. J. Dlugokencky, S. E. Michel, X. Lan, T. Röckmann, H. A. C. Denier Van Der Gon, J. Schmitt, P. I. Palmer, M. N. Dyonisius, Y. Oh, R. E. Fisher, D. Lowry,

J. L. France, J. W. C. White, G. Brailsford, T. Bromley, Atmospheric methane: Comparison between methane's record in 2006–2022 and during glacial terminations. *Global Biogeochem. Cycles* **37**, e2023GB007875 (2023).

9. X. Lan, S. Basu, S. Schwietzke, L. M. P. Bruhwiler, E. J. Dlugokencky, S. E. Michel, O. A. Sherwood, P. P. Tans, K. Thoning, G. Etiope, Q. Zhuang, L. Liu, Y. Oh, J. B. Miller, G. Pétron, B. H. Vaughn, M. Crippa, Improved constraints on global methane emissions and sinks using δ^{13}C-CH_4. *Global Biogeochem. Cycles* **35**, e2021GB007000 (2021).

10. Z. Zhang, B. Poulter, A. F. Feldman, Q. Ying, P. Ciais, S. Peng, X. Li, Recent intensification of wetland methane feedback. *Nat. Clim. Chang.* **13**, 430–433 (2023).

11. S. Peng, X. Lin, R. L. Thompson, Y. Xi, G. Liu, D. Hauglustaine, X. Lan, B. Poulter, M. Ramonet, M. Saunois, Y. Yin, Z. Zhang, B. Zheng, P. Ciais, Wetland emission and atmospheric sink changes explain methane growth in 2020. *Nature* **612**, 477–482 (2022).

12. Y. Oh, Q. Zhuang, L. R. Welp, L. Liu, X. Lan, S. Basu, E. J. Dlugokencky, L. Bruhwiler, J. B. Miller, S. E. Michel, S. Schwietzke, P. Tans, P. Ciais, J. P. Chanton, Improved global wetland carbon isotopic signatures support post-2006 microbial methane emission increase. *Commun Earth Environ* **3**, 159 (2022).

13. L. Feng, P. I. Palmer, R. J. Parker, M. F. Lunt, H. Bösch, Methane emissions are predominantly responsible for record-breaking atmospheric methane growth rates in 2020 and 2021. *Atmos. Chem. Phys.* **23**, 4863–4880 (2023).

14. A. Drinkwater, P. I. Palmer, L. Feng, T. Arnold, X. Lan, S. E. Michel, R. Parker, H. Boesch, Atmospheric data support a multi-decadal shift in the global methane budget towards natural tropical emissions. *Atmos. Chem. Phys.* **23**, 8429–8452 (2023).

15. Y. Zhu, K. J. Purdy, Ö. Eyice, L. Shen, S. F. Harpenslager, G. Yvon-Durocher, A. J. Dumbrell, M. Trimmer, Disproportionate increase in freshwater methane emissions induced by experimental warming. *Nat. Clim. Chang.* **10**, 685–690 (2020).

16. V. Gauci, E. Matthews, N. Dise, B. Walter, D. Koch, G. Granberg, M. Vile, Sulfur pollution suppression of the wetland methane source in the 20th and 21st centuries. *Proc. Natl. Acad. Sci. U.S.A.* **101**, 12583–12587 (2004).

17. K. J. van Groenigen, C. W. Osenberg, B. A. Hungate, Increased soil emissions of potent greenhouse gases under increased atmospheric CO_2. *Nature* **475**, 214–216 (2011).

18. E. N. Koffi, P. Bergamaschi, R. Alkama, A. Cescatti, An observation-constrained assessment of the climate sensitivity and future trajectories of wetland methane emissions. *Sci. Adv.* **6**, eaay4444 (2020).

19. Z. Zhang, N. E. Zimmermann, A. Stenke, X. Li, E. L. Hodson, G. Zhu, C. Huang, B. Poulter, Emerging role of wetland methane emissions in driving 21st century climate change. *Proc. Natl. Acad. Sci. U.S.A.* **114**, 9647–9652 (2017).

20. N. Gedney, C. Huntingford, E. Comyn-Platt, A. Wiltshire, Significant feedbacks of wetland methane release on climate change and the causes of their uncertainty. *Environ. Res. Lett.* **14**, 084027 (2019).

21. A. V. Eliseev, I. I. Mokhov, M. M. Arzhanov, P. F. Demchenko, S. N. Denisov, Interaction of the methane cycle and processes in wetland ecosystems in a climate model of intermediate complexity. *Izv. Atmos. Ocean. Phys.* **44**, 139–152 (2008).

22. D. T. Shindell, B. P. Walter, G. Faluvegi, Impacts of climate change on methane emissions from wetlands. *Geophys. Res. Lett.* **31**, L21202 (2004).

23. N. Gedney, Climate feedback from wetland methane emissions. *Geophys. Res. Lett.* **31**, L20503 (2004).

24. B. D. Stocker, R. Roth, F. Joos, R. Spahni, M. Steinacher, S. Zaehle, L. Bouwman, X.-R. , I. C. Prentice, Multiple greenhouse-gas feedbacks from the land biosphere under future climate change scenarios. *Nat. Clim. Change* **3**, 666–672 (2013).

25. E. Comyn-Platt, G. Hayman, C. Huntingford, S. E. Chadburn, E. J. Burke, A. B. Harper, W. J. Collins, C. P. Webber, T. Powell, P. M. Cox, N. Gedney, S. Sitch, Carbon budgets for 1.5

and 2 °C targets lowered by natural wetland and permafrost feedbacks. *Nat. Geosci.* **11**, 568–573 (2018).

26. C. Gudasz, D. Bastviken, K. Steger, K. Premke, S. Sobek, L. J. Tranvik, Temperature-controlled organic carbon mineralization in lake sediments. *Nature* **466**, 478–481 (2010).

27. G. Yvon-Durocher, A. P. Allen, D. Bastviken, R. Conrad, C. Gudasz, A. St-Pierre, N. Thanh-Duc, P. A. del Giorgio, Methane fluxes show consistent temperature dependence across microbial to ecosystem scales. *Nature* **507**, 488–491 (2014).

28. S. E. Chadburn, T. Aalto, M. Aurela, D. Baldocchi, C. Biasi, J. Boike, E. J. Burke, E. Comyn-Platt, A. J. Dolman, C. Duran-Rojas, Y. Fan, T. Friborg, Y. Gao, N. Gedney, M. Göckede, G. D. Hayman, D. Holl, G. Hugelius, L. Kutzbach, H. Lee, A. Lohila, F. W. Parmentier, T. Sachs, N. J. Shurpali, S. Westermann, Modeled microbial dynamics explain the apparent temperature sensitivity of wetland methane emissions. *Global Biogeochem. Cycles* **34**, e2020GB006678 (2020).

29. Y. Hu, X. Yue, C. Tian, H. Zhou, W. Fu, X. Zhao, Y. Zhao, Y. Chen, Identifying the main drivers of the spatiotemporal variations in wetland methane emissions during 2001–2020. *Front. Environ. Sci.* **11**, 1275742 (2023).

30. E. G. Nisbet, Climate feedback on methane from wetlands. *Nat. Clim. Chang.* **13**, 421–422 (2023).

31. W. J. Riley, Z. M. Subin, D. M. Lawrence, S. C. Swenson, M. S. Torn, L. Meng, N. M. Mahowald, P. Hess, Barriers to predicting changes in global terrestrial methane fluxes: Analyses using CLM4Me, a methane biogeochemistry model integrated in CESM. *Biogeosciences* **8**, 1925–1953 (2011).

32. X. Xu, F. Yuan, P. J. Hanson, S. D. Wullschleger, P. E. Thornton, W. J. Riley, X. Song, D. E. Graham, C. Song, H. Tian, Reviews and syntheses: Four decades of modeling methane cycling in terrestrial ecosystems. *Biogeosciences* **13**, 3735–3755 (2016).

33. H. Chen, X. Xu, C. Fang, B. Li, M. Nie, Differences in the temperature dependence of wetland CO_2 and CH4 emissions vary with water table depth. *Nat. Clim. Chang.* **11**, 766–771 (2021).

34. F. Murguia-Flores, V. J. Jaramillo, A. Gallego-Sala, Assessing methane emissions from tropical wetlands: Uncertainties from natural variability and drivers at the global scale. *Glob. Biogeochem.l Cycles* **37**, e2022GB007601 (2023).

35. E. M. Volodin, Methane cycle in the INM RAS climate model. *Izv. Atmos. Ocean. Phys.* **44**, 153–159 (2008).

36. D. R. Lovley, M. J. Klug, Sulfate reducers can outcompete methanogens at freshwater sulfate concentrations. *Appl. Environ. Microbiol.* **45**, 187–192 (1983).

37. M. R. Winfrey, J. G. Zeikus, Effect of sulfate on carbon and electron flow during microbial methanogenesis in freshwater sediments. *Appl. Environ. Microbiol.* **33**, 275–281 (1977).

38. P. Durack, K. Taylor, V. Eyring, S. Ames, C. Doutriaux, T. Hoang, D. Nadeau, M. Stockhause, P. Gleckler, "input4MIPs: Making [CMIP] model forcing more transparent" (LLNL-JRNL-729886, 1463030, 880514, 2017); https://doi.org/10.2172/1463030.

39. L. Deng, C. Huang, D. Kim, Z. Shangguan, K. Wang, X. Song, C. Peng, Soil GHG fluxes are altered by N deposition: New data indicate lower N stimulation of the N_2O flux and greater stimulation of the calculated C pools. *Glob Change Biol* **26**, 2613–2629 (2020).

40. J. Wu, X. Cheng, W. Xing, G. Liu, Soil-atmosphere exchange of CH4 in response to nitrogen addition in diverse upland and wetland ecosystems: A meta-analysis. *Soil Biol. Biochem.* **164**, 108467 (2022).

41. K. Banger, H. Tian, C. Lu, Do nitrogen fertilizers stimulate or inhibit methane emissions from rice fields? *Glob. Change Biol.* **18**, 3259–3267 (2012).

42. J. W. H. Dacey, B. G. Drake, M. J. Klug, Stimulation of methane emission by carbon dioxide enrichment of marsh vegetation. *Nature* **370**, 47–49 (1994).

43. Y. Lin, J. Yuan, D. Liu, H. Kang, C. Freeman, H.-W. Hu, G. Ye, W. Ding, Divergent responses of wetland methane emissions to elevated atmospheric CO_2 dependent on water table. *Water Res.* **205**, 117682 (2021).

44. H. Qian, Y. Jin, J. Chen, S. Huang, Y. Liu, J. Zhang, A. Deng, J. Zou, G. Pan, Y. Ding, Y. Jiang, K. J. van Groenigen, W. Zhang, Acclimation of CH4 emissions from paddy soil to atmospheric CO_2 enrichment in a growth chamber experiment. *Crop J* **10**, 140–146 (2022).

45. L. Möller, T. Sowers, M. Bock, R. Spahni, M. Behrens, J. Schmitt, H. Miller, H. Fischer, Independent variations of CH4 emissions and isotopic composition over the past 160,000 years. *Nat. Geosci.* **6**, 885–890 (2013).

46. W. J. Collins, J.-F. Lamarque, M. Schulz, O. Boucher, V. Eyring, M. I. Hegglin, A. Maycock, G. Myhre, M. Prather, D. Shindell, S. J. Smith, AerChemMIP: Quantifying the effects of chemistry and aerosols in CMIP6. *Geosci. Model Dev.* **10**, 585–607 (2017).

47. M. Meinshausen, Z. R. J. Nicholls, J. Lewis, M. J. Gidden, E. Vogel, M. Freund, U. Beyerle, C. Gessner, A. Nauels, N. Bauer, J. G. Canadell, J. S. Daniel, A. John, P. B. Krummel, G. Luderer, N. Meinshausen, S. A. Montzka, P. J. Rayner, S. Reimann, S. J. Smith, M. van den Berg, G. J. M. Velders, M. K. Vollmer, R. H. J. Wang, The shared socio-economic pathway (SSP) greenhouse gas concentrations and their extensions to 2500. *Geosci. Model Dev.* **13**, 3571–3605 (2020).

48. W. Cheng, L. Dan, X. Deng, J. Feng, Y. Wang, J. Peng, J. Tian, W. Qi, Z. Liu, X. Zheng, D. Zhou, S. Jiang, H. Zhao, X. Wang, Global monthly gridded atmospheric carbon dioxide concentrations under the historical and future scenarios. *Sci. Data* **9**, 83 (2022).

49. A. A. Bloom, K. W. Bowman, M. Lee, A. J. Turner, R. Schroeder, J. R. Worden, R. Weidner, K. C. McDonald, D. J. Jacob, A global wetland methane emissions and uncertainty dataset for atmospheric chemical transport models (WetCHARTs version 1.0). *Geosci. Model Dev.* **10**, 2141–2156 (2017).

50. S. Ma, J. R. Worden, A. A. Bloom, Y. Zhang, B. Poulter, D. H. Cusworth, Y. Yin, S. Pandey, J. D. Maasakkers, X. Lu, L. Shen, J. Sheng, C. Frankenberg, C. E. Miller, D. J. Jacob,

Satellite constraints on the latitudinal distribution and temperature sensitivity of wetland methane emissions. *AGU Adv.* **2**, e2021AV000408 (2021).

51. L. Shen, D. J. Jacob, R. Gautam, M. Omara, T. R. Scarpelli, A. Lorente, D. Zavala-Araiza, X. Lu, Z. Chen, J. Lin, National quantifications of methane emissions from fuel exploitation using high resolution inversions of satellite observations. *Nat. Commun.* **14**, 4948 (2023).

52. B. Zhang, H. Tian, C. Lu, G. Chen, S. Pan, C. Anderson, B. Poulter, Methane emissions from global wetlands: An assessment of the uncertainty associated with various wetland extent data sets. *Atmos. Environ.* **165**, 310–321 (2017).

53. C. Gerlein-Safdi, A. A. Bloom, G. Plant, E. A. Kort, C. S. Ruf, Improving representation of tropical wetland methane emissions with CYGNSS inundation maps. *Global Biogeochem. Cycles* **35**, e2020GB006890 (2021).

54. S. Calabrese, A. Garcia, J. L. Wilmoth, X. Zhang, A. Porporato, Critical inundation level for methane emissions from wetlands. *Environ. Res. Lett.* **16**, 044038 (2021).

55. K. Chang, W. J. Riley, N. Collier, G. McNicol, E. Fluet-Chouinard, S. H. Knox, K. B. Delwiche, R. B. Jackson, B. Poulter, M. Saunois, N. Chandra, N. Gedney, M. Ishizawa, A. Ito, F. Joos, T. Kleinen, F. Maggi, J. McNorton, J. R. Melton, P. Miller, Y. Niwa, C. Pasut, P. K. Patra, C. Peng, S. Peng, A. Segers, H. Tian, A. Tsuruta, Y. Yao, Y. Yin, W. Zhang, Z. Zhang, Q. Zhu, Q. Zhu, Q. Zhuang, Observational constraints reduce model spread but not uncertainty in global wetland methane emission estimates. *Glob. Change Biol.* **29**, 4298–4312 (2023).

56. V. Gauci, V. Figueiredo, N. Gedney, S. R. Pangala, T. Stauffer, G. P. Weedon, A. Enrich-Prast, Non-flooded riparian Amazon trees are a regionally significant methane source. *Phil. Trans. R. Soc. A.* **380**, 20200446 (2022).

57. J. T. Shaw, G. Allen, P. Barker, J. R. Pitt, D. Pasternak, S. J.-B. Bauguitte, J. Lee, K. N. Bower, M. C. Daly, M. F. Lunt, A. L. Ganesan, A. R. Vaughan, F. Chibesakunda, M. Lambakasa, R. E. Fisher, J. L. France, D. Lowry, P. I. Palmer, S. Metzger, R. J. Parker, N. Gedney, P. Bateson, M. Cain, A. Lorente, T. Borsdorff, E. G. Nisbet, Large methane emission

fluxes observed from tropical wetlands in Zambia. *Global Biogeochem. Cycles* **36**, e2021GB007261 (2022).

58. G. Muyzer, A. J. M. Stams, The ecology and biotechnology of sulphate-reducing bacteria. *Nat. Rev. Microbiol.* **6**, 441–454 (2008).

59. C. P. Boardman, V. Gauci, A. Fox, S. Blake, D. J. Beerling, Reduction of the temperature sensitivity of minerotrophic fen methane emissions by simulated glacial atmospheric carbon dioxide starvation. *J. Geophys. Res. Biogeosci.* **118**, 462–470 (2013).

60. J. Ehleringer, O. Björkman, Quantum yields for CO_2 uptake in C_3 and C_4 plants: Dependence on temperature, CO_2, and O_2 concentration. *Plant Physiol.* **59**, 86–90 (1977).

61. R. F. Sage, D. S. Kubien, The temperature response of C_3 and C_4 photosynthesis. *Plant Cell Environ.* **30**, 1086–1106 (2007).

62. C. J. Still, J. A. Berry, G. J. Collatz, R. S. DeFries, Global distribution of C_3 and C_4 vegetation: Carbon cycle implications. *Global Biogeochem. Cycles* **17**, 6.1–6.14 (2003).

63. E. J. Burke, Y. Zhang, G. Krinner, Evaluating permafrost physics in the Coupled Model Intercomparison Project 6 (CMIP6) models and their sensitivity to climate change. *Cryosphere* **14**, 3155–3174 (2020).

64. G. J. Collatz, J. A. Berry, J. S. Clark, Effects of climate and atmospheric CO_2 partial pressure on the global distribution of C 4 grasses: Present, past, and future. *Oecologia* **114**, 441–454 (1998).

65. J. A. Morgan, D. R. LeCain, E. Pendall, D. M. Blumenthal, B. A. Kimball, Y. Carrillo, D. G. Williams, J. Heisler-White, F. A. Dijkstra, M. West, C_4 grasses prosper as carbon dioxide eliminates desiccation in warmed semi-arid grassland. *Nature* **476**, 202–205 (2011).

66. T. Weber, N. A. Wiseman, A. Kock, Global ocean methane emissions dominated by shallow coastal waters. *Nat. Commun.* **10**, 4584 (2019).

67. R. A. Alvarez, D. Zavala-Araiza, D. R. Lyon, D. T. Allen, Z. R. Barkley, A. R. Brandt, K. J. Davis, S. C. Herndon, D. J. Jacob, A. Karion, E. A. Kort, B. K. Lamb, T. Lauvaux, J. D. Maasakkers, A. J. Marchese, M. Omara, S. W. Pacala, J. Peischl, A. L. Robinson, P. B. Shepson, C. Sweeney, A. Townsend-Small, S. C. Wofsy, S. P. Hamburg, Assessment of methane emissions from the U.S. oil and gas supply chain. *Science* **361**, 186–188 (2018).

68. T. R. Scarpelli, D. J. Jacob, S. Grossman, X. Lu, Z. Qu, M. P. Sulprizio, Y. Zhang, F. Reuland, D. Gordon, J. R. Worden, Updated Global Fuel Exploitation Inventory (GFEI) for methane emissions from the oil, gas, and coal sectors: Evaluation with inversions of atmospheric methane observations. *Atmos. Chem. Phys.* **22**, 3235–3249 (2022).

69. European Commission and USA, About the Global Methane Pledge (2021), www.globalmethanepledge.org [accessed December 2023].

70. V. Gauci, N. Dise, S. Blake, Long-term suppression of wetland methane flux following a pulse of simulated acid rain. *Geophys. Res. Lett.* **32**, L12804 (2005).

71. M. Guimberteau, D. Zhu, F. Maignan, Y. Huang, C. Yue, S. Dantec-Nédélec, C. Ottlé, A. Jornet-Puig, A. Bastos, P. Laurent, D. Goll, S. Bowring, J. Chang, B. Guenet, M. Tifafi, S. Peng, G. Krinner, A. Ducharne, F. Wang, T. Wang, X. Wang, Y. Wang, Z. Yin, R. Lauerwald, E. Joetzjer, C. Qiu, H. Kim, P. Ciais, ORCHIDEE-MICT (v8.4.1), a land surface model for the high latitudes: Model description and validation. *Geosci. Model Dev.* **11**, 121–163 (2018).

72. T. F. Keenan, X. Luo, B. D. Stocker, M. G. De Kauwe, B. E. Medlyn, I. C. Prentice, N. G. Smith, C. Terrer, H. Wang, Y. Zhang, S. Zhou, A constraint on historic growth in global photosynthesis due to rising CO2. *Nat. Clim. Chang.* **13**, 1376–1381 (2023).

73. H. A. Denier Van Der Gon, P. M. Van Bodegom, R. Wassmann, R. S. Lantin, T. M. Metra-Corton, Sulfate-containing amendments to reduce methane emissions from rice fields: Mechanisms, effectiveness and costs. *Mitig. Adapt. Strat. Glob. Chang.* **6**, 71–89 (2001).

74. V. Gauci, N. B. Dise, G. Howell, M. E. Jenkins, Suppression of rice methane emission by sulfate deposition in simulated acid rain. *J. Geophys. Res.* **113**, 2007JG000501 (2008).

75. E. Salmon, F. Jégou, B. Guenet, L. Jourdain, C. Qiu, V. Bastrikov, C. Guimbaud, D. Zhu, P. Ciais, P. Peylin, S. Gogo, F. Laggoun-Défarge, M. Aurela, M. S. Bret-Harte, J. Chen, B. H. Chojnicki, H. Chu, C. W. Edgar, E. S. Euskirchen, L. B. Flanagan, K. Fortuniak, D. Holl, J. Klatt, O. Kolle, N. Kowalska, L. Kutzbach, A. Lohila, L. Merbold, W. Pawlak, T. Sachs, K. Ziemblińska, Assessing methane emissions for northern peatlands in ORCHIDEE-PEAT revision 7020. *Geosci. Model Dev.* **15**, 2813–2838 (2022).

76. P. Bergamaschi, S. Houweling, A. Segers, M. Krol, C. Frankenberg, R. A. Scheepmaker, E. Dlugokencky, S. C. Wofsy, E. A. Kort, C. Sweeney, T. Schuck, C. Brenninkmeijer, H. Chen, V. Beck, C. Gerbig, Atmospheric CH_4 in the first decade of the 21st century: Inverse modeling analysis using SCIAMACHY satellite retrievals and NOAA surface measurements. *J. Geophys. Res. Atmos.* **118**, 7350–7369 (2013).

77. R. Gelaro, W. McCarty, M. J. Suárez, R. Todling, A. Molod, L. Takacs, C. A. Randles, A. Darmenov, M. G. Bosilovich, R. Reichle, K. Wargan, L. Coy, R. Cullather, C. Draper, S. Akella, V. Buchard, A. Conaty, A. M. Da Silva, W. Gu, G.-K. Kim, R. Koster, R. Lucchesi, D. Merkova, J. E. Nielsen, G. Partyka, S. Pawson, W. Putman, M. Rienecker, S. D. Schubert, M. Sienkiewicz, B. Zhao, The modern-era retrospective analysis for research and applications, version 2 (MERRA-2). *J. Climate* **30**, 5419–5454 (2017).

78. S. E. Nicholson, Long-term variability of the East African ‘short rains’ and its links to large-scale factors. *Intl Journal of Climatology* **35**, 3979–3990 (2015).

79. S. Pandey, S. Houweling, M. Krol, I. Aben, G. Monteil, N. Nechita-Banda, E. J. Dlugokencky, R. Detmers, O. Hasekamp, X. Xu, W. J. Riley, B. Poulter, Z. Zhang, K. C. McDonald, J. W. C. White, P. Bousquet, T. Röckmann, Enhanced methane emissions from tropical wetlands during the 2011 La Niña. *Sci. Rep.* **7**, 45759 (2017).

80. V. Eyring, S. Bony, G. A. Meehl, C. A. Senior, B. Stevens, R. J. Stouffer, K. E. Taylor, Overview of the Coupled Model Intercomparison Project Phase 6 (CMIP6) experimental design and organization. *Geosci. Model Dev.* **9**, 1937–1958 (2016).

81. L. Shen, L. J. Mickley, L. T. Murray, Influence of 2000–2050 climate change on particulate matter in the United States: Results from a new statistical model. *Atmos. Chem. Phys.* **17**, 4355–4367 (2017).

82. Z. Zhang, E. Fluet-Chouinard, K. Jensen, K. McDonald, G. Hugelius, T. Gumbricht, M. Carroll, C. Prigent, A. Bartsch, B. Poulter, Development of the global dataset of Wetland Area and Dynamics for Methane Modeling (WAD2M). *Earth Syst. Sci. Data* **13**, 2001–2023 (2021).

83. G. McNicol, E. Fluet-Chouinard, Z. Ouyang, S. Knox, Z. Zhang, T. Aalto, S. Bansal, K. Chang, M. Chen, K. Delwiche, S. Feron, M. Goeckede, J. Liu, A. Malhotra, J. R. Melton, W. Riley, R. Vargas, K. Yuan, Q. Ying, Q. Zhu, P. Alekseychik, M. Aurela, D. P. Billesbach, D. I. Campbell, J. Chen, H. Chu, A. R. Desai, E. Euskirchen, J. Goodrich, T. Griffis, M. Helbig, T. Hirano, H. Iwata, G. Jurasinski, J. King, F. Koebsch, R. Kolka, K. Krauss, A. Lohila, I. Mammarella, M. Nilson, A. Noormets, W. Oechel, M. Peichl, T. Sachs, A. Sakabe, C. Schulze, O. Sonnentag, R. C. Sullivan, E. Tuittila, M. Ueyama, T. Vesala, E. Ward, C. Wille, G. X. Wong, D. Zona, L. Windham-Myers, B. Poulter, R. B. Jackson, Upscaling wetland methane emissions from the FLUXNET-CH4 Eddy covariance network (UpCH4 v1.0): Model development, network assessment, and budget comparison. *AGU Adv.* **4**, e2023AV000956 (2023).

84. M. J. Gidden, K. Riahi, S. J. Smith, S. Fujimori, G. Luderer, E. Kriegler, D. P. van Vuuren, M. van den Berg, L. Feng, D. Klein, K. Calvin, J. C. Doelman, S. Frank, O. Fricko, M. Harmsen, T. Hasegawa, P. Havlik, J. Hilaire, R. Hoesly, J. Horing, A. Popp, E. Stehfest, K. Takahashi, Global emissions pathways under different socioeconomic scenarios for use in CMIP6: A dataset of harmonized emissions trajectories through the end of the century. *Geosci. Model Dev.* **12**, 1443–1475 (2019).

85. A. J. Cannon, S. R. Sobie, T. Q. Murdock, Bias correction of gcm precipitation by quantile mapping: How well do methods preserve changes in quantiles and extremes? *J. Climate* **28**, 6938–6959 (2015).

86. IPCC, *Climate Change 2021: The Physical Science Basis. Contribution of Working Group I to the Sixth Assessment Report of the Intergovernmental Panel on Climate Change*, V.

Masson-Delmotte, P. Zhai, A. Pirani, S. L. Connors, C. Péan, S. Berger, N. Caud, Y. Chen, L. Goldfarb, M. I. Gomis, M. Huang, K. Leitzell, E. Lonnoy, J. B. R. Matthews, T. K. Maycock, T. Waterfield, O. Yelekçi, R. Yu and B. Zhou, Eds. (Cambridge Univ. Press, 2021).

87. M. Pester, Sulfate-reducing microorganisms in wetlands – fameless actors in carbon cycling and climate change. *Front. Microbio.* **3**, 72 (2012).

88. A. J. M. Stams, S. J. W. H. O. Elferink, P. Westermann, "Metabolic Interactions Between Methanogenic Consortia and Anaerobic Respiring Bacteria" in *Biomethanation I*, B. K. Ahring, I. Angelidaki, E. C. de Macario, H. N. Gavala, J. Hofman-Bang, A. J. L. Macario, S. J. W. H. O. Elferink, L. Raskin, A. J. M. Stams, P. Westermann, D. Zheng, Eds. (Springer, 2003), pp. 31–56.

89. R. Wania, J. R. Melton, E. L. Hodson, B. Poulter, B. Ringeval, R. Spahni, T. Bohn, C. A. Avis, G. Chen, A. V. Eliseev, P. O. Hopcroft, W. J. Riley, Z. M. Subin, H. Tian, P. M. van Bodegom, T. Kleinen, Z. C. Yu, J. S. Singarayer, S. Zürcher, D. P. Lettenmaier, D. J. Beerling, S. N. Denisov, C. Prigent, F. Papa, J. O. Kaplan, Present state of global wetland extent and wetland methane modelling: Methodology of a model inter-comparison project (WETCHIMP). *Geosci. Model Dev.* **6**, 617–641 (2013).

90. D. Yan, K. Wang, T. Qin, B. Weng, H. Wang, W. Bi, X. Li, M. Li, Z. Lv, F. Liu, S. He, J. Ma, Z. Shen, J. Wang, H. Bai, Z. Man, C. Sun, M. Liu, X. Shi, L. Jing, R. Sun, S. Cao, C. Hao, L. Wang, M. Pei, B. Dorjsuren, M. Gedefaw, A. Girma, A. Abiyu, A data set of global river networks and corresponding water resources zones divisions. *Sci. Data* **6**, 219 (2019).

91. A. L. Ganesan, A. C. Stell, N. Gedney, E. Comyn-Platt, G. Hayman, M. Rigby, B. Poulter, E. R. C. Hornibrook, Spatially resolved isotopic source signatures of wetland methane emissions. *Geophys. Res. Lett.* **45**, 3737–3745 (2018).

92. B. Ringeval, P. Friedlingstein, C. Koven, P. Ciais, N. de Noblet-Ducoudré, B. Decharme, P. Cadule, Climate-CH_4 feedback from wetlands and its interaction with the climate-CO_2 feedback. *Biogeosciences* **8**, 2137–2157 (2011).

93. M. J. Prather, C. D. Holmes, J. Hsu, Reactive greenhouse gas scenarios: Systematic exploration of uncertainties and the role of atmospheric chemistry. *Geophys. Res. Lett.* **39**, 2012GL051440 (2012).

94. United Nations Environment Programme and Climate and Clean Air Coalition, "Global methane assessment: Benefits and costs of mitigating methane emissions" (Publication 978-92-807-3854-4, 2021); https://wedocs.unep.org/bitstream/handle/20.500.11822/35913/GMA.pdf.